People`s Democratic Republic of Algeria
Ministry of Higher Education and Scientific Research
University of Echahid Hamma Lakhdar - El Oued
Faculty of Technology
Department of Electrical Engineering

Dissertation

ACADEMIC MASTER

Domain: Science and Technology

Division: Electrical Engineering.

Specialty: **Electrical Control**.

Presented by:

Said ZAOUCHE

Mohammed Lazhar SAI

Mohammed Tahar BAKKOUCHE

Entitled:

Predictive Control of induction motor drive for PV array water pumping under varying environmental conditions

Publicly defended in: 28/05 /2025

Board of Examiners:

Dr. Said CHIKHA	**Chairman**
Dr. Ridha KECHIDA	**Supervisor**
Dr. Abdelmalek GACEM.	**Examiner**

Academic Year: 2024/2025

ملخص:

في ظل التزايد المستمر في الطلب على مصادر الطاقة المستدامة، أصبحت أنظمة الطاقة الشمسية من بين الحلول الأكثر فاعلية لتلبية احتياجات المجتمعات من الكهرباء، خاصة في المناطق الريفية والنائية. ومن أبرز التطبيقات الحيوية للطاقة الشمسية، أنظمة ضخ المياه، التي تُستخدم لأغراض الزراعة وتوفير مياه الشرب.

تُستخدم **المحركات الحثية** في هذه الأنظمة نظرًا لكفاءتها العالية وموثوقيتها، إلا أن تشغيلها بالاعتماد على الطاقة الشمسية يواجه تحديات تقنية نتيجة التقلبات البيئية المستمرة مثل الإشعاع الشمسي ودرجة الحرارة، مما يسبب تغيرًا في القدرة الخارجة من الألواح الكهروضوئية. لمعالجة هذه التحديات، تقترح هذه الدراسة تطبيق **التحكم التنبؤي النموذجي(PTC) "Predictive Torque Control "** كحل ذكي ومتطور للتحكم في قيادة المحرك الحثي، بهدف تحقيق أداء مستقر وكفء تحت ظروف تشغيل متغيرة. يعتمد هذا النوع من التحكم على نماذج رياضية دقيقة للتنبؤ بسلوك النظام واختيار أفضل إجراء في كل لحظة زمنية، مما يجعله مثاليًا للأنظمة غير الخطية.

تتناول الدراسة تحليل الأداء الديناميكي للنظام تحت ظروف مناخية مختلفة، وتوضح كيف يُسهم دمج تقنيات التحكم الذكية مثل PTC في تحسين الكفاءة التشغيلية والتكيف السريع مع التغيرات البيئية.

الكلمات المفتاحية:

التحكم التنبؤي النموذجي(PTC) ، الطاقة الشمسية، الألواح الكهروضوئية، محول رافع للجهد، تتبع نقطة القدرة العظمى (MPPT)، خوارزمية P&O ، خوارزمية INC ، المحرك الحثي، مضخة الطرد المركزي، العاكس(VSI)

Abstract

Against the backdrop of growing global demand for sustainable energy solutions, photovoltaic systems have emerged as one of the most effective approaches for meeting electricity needs particularly in rural and remote communities. Among their most vital applications are solar-powered water pumping systems, which serve critical agricultural irrigation and potable water supply functions.

These systems predominantly employ induction motors due to their proven reliability and operational efficiency. However, their solar-dependent operation presents distinct technical challenges stemming from continuous environmental variability, particularly fluctuations in solar irradiance and ambient temperature that directly impact photovoltaic output power characteristics. To address these challenges, this study proposes the implementation of **Predictive Torque Control (PTC)** as an intelligent, advanced control strategy for induction motor drives. This model-based predictive control approach leverages precise mathematical

modeling to forecast system behavior and optimize real-time control actions, making it particularly suitable for nonlinear systems operating under variable conditions.

The research comprehensively analyzes the system's dynamic performance across diverse climatic scenarios, demonstrating how intelligent control integration specifically PTC enhances operational efficiency while ensuring rapid adaptation to environmental transients. Key findings highlight the control strategy's capability to maintain stable performance despite photovoltaic power fluctuations.

Keywords:

Predictive Torque Control (PTC), solar energy, photovoltaic panels, boost converter, Maximum Power Point Tracking (MPPT), P&O algorithm, INC algorithm, induction motor, centrifugal pump, voltage source inverter (VSI).

List of Abbreviations

AC: Alternative Current.

DC: Direct Current.

MPC: Model Predictive Control.

GPV: generator Photovoltaic.

MPP: Maximum Power Point

MPPT: Maximum PowerPoint Tracking.

P&O: Perturb and Observe.

PWM: Pulse Width Modulation.

PV: Photovoltaic.

SPWM: Sinusoidal Pulse Width Modulation.

STC: Standard Test Conditions

VSI: Voltage Source Inverter.

Ipv: Current of the photovoltaic panel

Vpv: Voltage of the photovoltaic panel

Ppv: Power of the photovoltaic panel

Icc: Short circuit current

Vco: Open circuit voltage

Is: the saturation current

iph: Current delivered by the cell

vph: Voltage at the output of the cell

id: Current flowing through the diode

vd: Voltage across the diode

rs: Series resistor

rp: Parallel resistance

a: the ideality factor of Junction $1<n<3$

Kb: Boltzmann constant (1 ,38.10-23 J/K)

T: temperature of the cell in degrees kelvin

q: Electron charge (1,602.10-19)

Vsabc: Stator voltages

Vrabc: Rotor voltages

Isabc: Stator currents

Irabc: Rotor currents

Φsabc: Stator Fluxs

Φrabc: Rotor Fluxs

Lss : matrix of stator inductors

Lrr : matrix of rotor inductors

Rs.Rr: Stator and rotor resistances respectively

Ls. Lr: Stator and rotor inductances respectively

Msr : Stator-rotor mutual inductance

ms : Mutual inductance between stator phases.

mr : Mutual inductance between rotor phases.

θ : Flux angle

(α , β): stator Axes

P: Number of poles pairs

Tem: electromagnetic torque

J: moment of inertia of the rotating masses

f: viscous friction coefficient

Ωr: Speed of rotation of the machine

σ: Blondel's coefficient

[A] : Transition matrix.

[B] : Command matrix.

[P] : PARK transformation matrix.

φ: The water flow (m^3/s)

H: The total height (m)

ω: Rotation speed (rad/s)

Hg : is the geodesic height (m)

Vs : Effective value of the voltage.

Te : Sampling period.

Sabc : Boolean control values of the inverter arms.

ξ : Damping Coefficient.

Table of contents

Chapter IV: Predictive Torque Control (PTC) of Induction Motor

General Introduction

The global energy landscape has undergone profound transformation in recent decades, characterized by unprecedented industrialization and escalating energy demands. This paradigm shift presents a dual challenge: while energy remains fundamental to economic development, the predominant reliance on finite fossil resources (including coal, petroleum, and uranium) raises critical sustainability concerns. These non-renewable reserves not only face inevitable depletion given their geological formation timescales vastly exceeding consumption rates but also contribute significantly to environmental degradation through greenhouse gas emissions and climate change acceleration.

This urgent context necessitates a fundamental restructuring of global energy systems, transitioning from exhaustible resources to sustainable alternatives. Among renewable solutions, solar energy has emerged as particularly strategic due to three key advantages: essentially inexhaustible availability, minimal environmental impact during operation, and continuous technological improvements driving cost reductions. These characteristics position photovoltaic technology as a cornerstone of sustainable energy infrastructure.

A compelling demonstration of solar energy's practical viability appears in photovoltaic water pumping systems. These systems exemplify the successful displacement of conventional fuel-powered pumps, offering both ecological benefits and long-term economic advantages—particularly in agricultural and remote community applications where grid connectivity is limited. The transition to such renewable-powered systems represents not merely an environmental imperative, but increasingly, an economically rational energy solution.

This study focuses on the design and implementation of a solar photovoltaic water pumping system that utilizes **Predictive Torque Control (PTC)** as the control strategy for managing the operation of an induction motor that drives a centrifugal pump. The system is used to extract groundwater and store it, meeting water demands in locations that are not connected to conventional electrical infrastructure.

Chapter One provides a theoretical background on photovoltaic water pumping systems, detailing their components and operation, and presenting key concepts related to their design.

Chapter Two addresses the mathematical modeling of the PV array and the boost converter, incorporating Maximum Power Point Tracking (MPPT) techniques through algorithms such as Perturb and Observe (P&O) and Incremental Conductance (INC).

Chapter Three presents detailed modeling of the system's essential components, starting with the induction motor, followed by the application of the Park transformation to simplify analysis, and ending with models of the centrifugal pump and voltage source inverter.

Finally, Chapter Four is dedicated to explaining the principles of Model Predictive Torque Control (PTC), its integration into the proposed system, and its impact on improving dynamic performance and efficiency. The chapter also presents and analyzes simulation results under various operating conditions.

Chapter I.
Photovoltaic pumping systems

I.1. Introduction

Photovoltaic energy is the direct transformation of sunlight into electrical energy through cells that rely on a physical phenomenon known as the photovoltaic effect. This effect generates an electromotive force when the surface of the cell is exposed to light. The term "photovoltaic" is derived from the Greek word "photo," meaning light, and "voltaic," which comes from the name of the Italian physicist *Alessandro Volta* (1754–1827), who greatly contributed to the discovery of electricity. Thus, photovoltaic essentially means "light electricity." In this section, we will discuss the general concepts of solar energy, the equivalent model of a photovoltaic cell, and the details of a photovoltaic generator.

I.2. History

The development of photovoltaic systems has been the result of continuous work over many years, with contributions from various scientists throughout history. Some key milestones include:

- **1839**: French physicist *Antoine Becquerel* discovers the photovoltaic effect.
- **1875**: *Werner Von Siemens* presents a paper on the photovoltaic effect in semiconductors to the Berlin Academy of Sciences.
- **1887**: *Heinrich Rudolf Hertz* understands and presents the photoelectric effect, publishing his findings in the scientific journal *Annalen der Physik*.
- **1905**: *Albert Einstein* explains the photoelectric phenomenon, which leads to him receiving the *Nobel Prize* in Physics in 1921.
- **1954**: American researchers *Chapin, Pearson*, and *Prince from Bell Laboratories* develop the first silicon photovoltaic cell, achieving 4% efficiency, at a time when the emerging space industry seeks ways to power satellites.
- **1958**: A photovoltaic cell with 9% efficiency is developed. The first *Vanguard* satellites, powered by photovoltaic cells, are launched into space.
- **1973**: The first house powered by photovoltaic cells is built at the University of Wilmington in Delaware, USA.
- **1983**: The first car powered by photovoltaic energy travels 4,000 km in Australia.
- **1995**: Photovoltaic rooftop programs connected to the grid are launched in Japan and Germany, becoming more widespread from 2001.
- **2000**: The EEG Renewable Energy Sources Act (EEG), implemented on April 1, 2000, and amended in 2004 and 2009, is the result of the transposition of the European directive to promote renewable energies in the electricity sector.

- **2005**: In December 2005, the first photovoltaic solar power plant of the Prime Energy group was connected to the grid in Weil am Rhein (Baden-Württemberg), Hagen Heimer Strasse 17, 79576 Weil am Rhein [1].

This discovery, later called the "photoelectric effect," had a significant impact on the development of photovoltaic panels.

I.3. The Photovoltaic Effect

The photovoltaic effect is a process that transforms energy emitted by the sun, in the form of photons, into electrical energy using a semiconductor component called a solar cell. The photovoltaic effect can only occur if there is a potential barrier within the semiconductor before it is illuminated. Such a barrier exists at the interface between two differently doped volumes, meaning where two types of impurities with different concentrations have been introduced, for example, a P-N type. When this material is illuminated, the electric charges, made mobile by the light (photoelectric effect), will be separated by the barrier, with positive charges on one side and negative charges on the other [2]. Among the most commonly used semiconductor materials are silicon, germanium, gallium sulfide, and gallium arsenide.

I.4. The Photovoltaic Cell:

The photovoltaic cell is an electronic component that generates electricity when exposed to light (photons), through the photovoltaic effect. A PV cell, therefore, is a device that allows the transformation of solar energy into electrical energy. This transformation is based on the following three mechanisms:

- **Absorption of photons** (whose energy is greater than the bandgap) by the material constituting the device.
- **Conversion of the photon energy into electrical energy**, which corresponds to the creation of electron-hole pairs in the semiconductor material.
- **Collection of the generated particles** in the device.

The material making up the PV cell must possess two energy levels and be conductive enough to allow current flow. An electric field is necessary to separate the electron-hole pairs created. For this, a P-N junction is most commonly used [3].

❖ **Semiconductors:** Semiconductors are materials whose conductivity lies between that of conductors and insulators. Unlike conductors and insulators, the conductivity of semiconductors strongly depends on their purity, structural irregularities, temperature, and other physical and chemical factors. This property is their main advantage, as it allows the construction of most electronic components with highly diverse characteristics.

I.4.1. Doping of Semiconductors: Doping a material involves introducing atoms of another material into its matrix. These atoms will replace some of the original atoms, thereby introducing more electrons or holes. The dopant atoms are also called impurities and are present in a diluted phase: their concentration remains negligible compared to that of the atoms of the original material. In an intrinsic or pure semiconductor, there are no dopant atoms. All the electrons present in the conduction band come from the valence band. Therefore, there are as many electrons as there are holes: n = p = ni. where ni is the intrinsic concentration. Any doping serves to modify this balance between electrons and holes, favoring electrical conduction through one of the two types of carriers. There are two types of doping:

A. N-type Doping: Figure I.1 represents N-type doping, which involves adding a phosphorus atom to the silicon crystal structure. Phosphorus, with five electrons in its outer electron shell, will bond with four silicon atoms, leaving one electron free. This addition gives the crystal structure an overall negative charge [2].

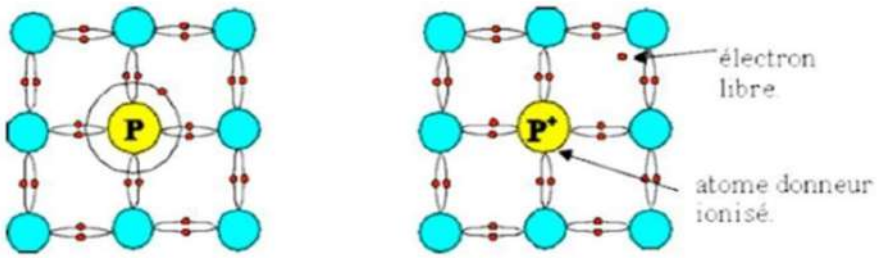

Fig I.1: N-type Doping

B. P-type Doping: figure I.2 represents P-type doping, which involves adding a boron atom to the silicon crystal structure. Boron, having three electrons in its outer electron shell, will bond with four silicon atoms, thus leaving a hole free. This addition results in giving the crystal structure an overall positive charge [2].

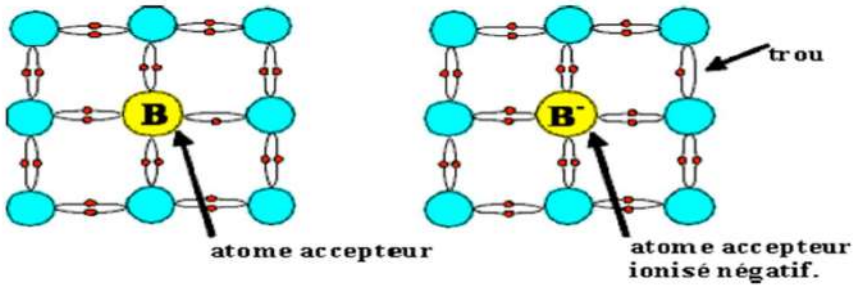

Fig I.2: P-type Doping

I.4.2. P-N Junction:

The P-N junction is the basis of most semiconductor applications. It is created by bringing a P-type semiconductor into contact with an N-type semiconductor (theoretically). In the contact zone, the free electrons from the N region enter the P region and recombine with the holes. Similarly, the holes from the P region enter the N region and recombine with the electrons. This phenomenon

is called diffusion. As a result, at the transition between the regions, a zone devoid of mobile charges appears, called the **depletion region** (also known as the **space charge region**), where only the fixed impurity atoms remain (acceptor ions in the P region, donor ions in the N region) along with neutral semiconductor atoms. The charges formed by the fixed ions give rise to an electric field **E** in the depletion region, and consequently, a potential difference $\mathbf{V_0}$ (called the potential barrier) across this region. This region has high impedance. The electric field **E** tends to keep the majority carriers in their respective regions and opposes the cause that gives rise to it, leading to an equilibrium state [4]. This phenomenon is represented in figure I.3.

However, the electric field **E** does not prevent the passage of minority carriers present in the P and N regions (the "saturation" current $\mathbf{I_{sat}}$). This movement is balanced by the majority carriers, who possess the energy necessary to overcome the potential barrier.

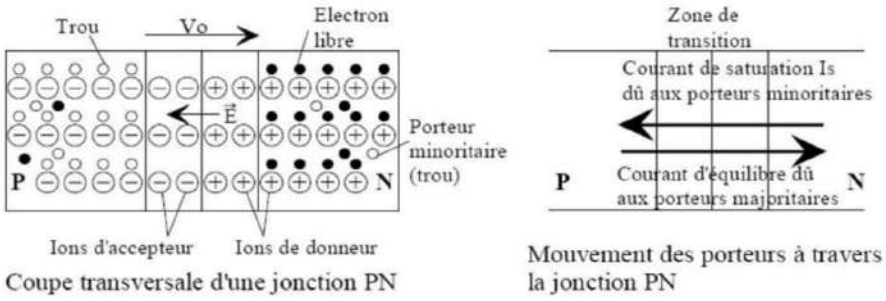

Fig I.3: P-N Junction**.**

I.4.3 Operating Principle:

The photovoltaic effect used in solar cells allows the direct conversion of light energy from solar rays into electricity through the production and transport of positive and negative electric charges in a semiconductor material under the effect of light. This material consists of two parts: one with an excess of electrons, called N-doped, and the other with a deficiency of electrons, called P-doped.

When the first part is brought into contact with the second, the excess electrons in the N material diffuse into the P material. The initially N-doped region becomes positively charged, and the initially P-doped region becomes negatively charged. Thus, an electric field is created between them, which tends to push the electrons into the N region and the holes into the P region. A P-N junction is formed. By adding metal contacts to the N and P regions, a diode is obtained. When the junction is illuminated, photons with energy equal to or greater than the bandgap transfer their energy to the atoms, causing each electron to move from the valence band to the conduction band, leaving behind a hole capable of moving, thus creating an electron-hole pair. If a load is placed across the cell, the electrons from the N region join the holes in the P region via the external

connection, generating a potential difference and allowing the electric current to flow. Figure I.4 represents the principle of PV conversion [2].

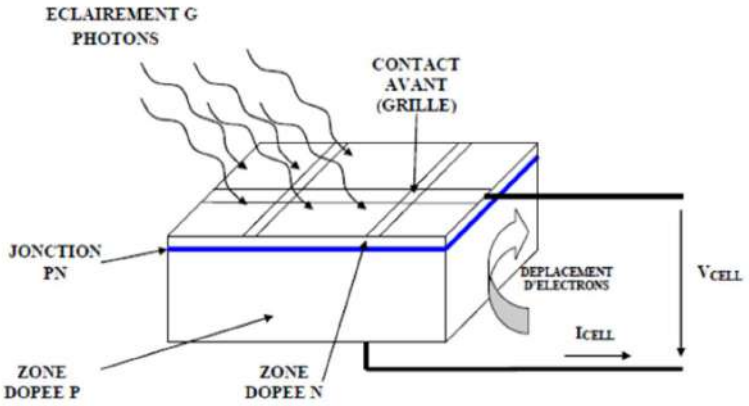

Fig I.4: Operating Principle of a Solar Cell

I.4.4 Different Types of Cells: There are several types of cells based on the microscopic structure of silicon (Figure I.5):

- **Monocrystalline Silicon Cell** (a)
- **Polycrystalline Silicon Cell** (b)
- **Amorphous Silicon Cell** (c)

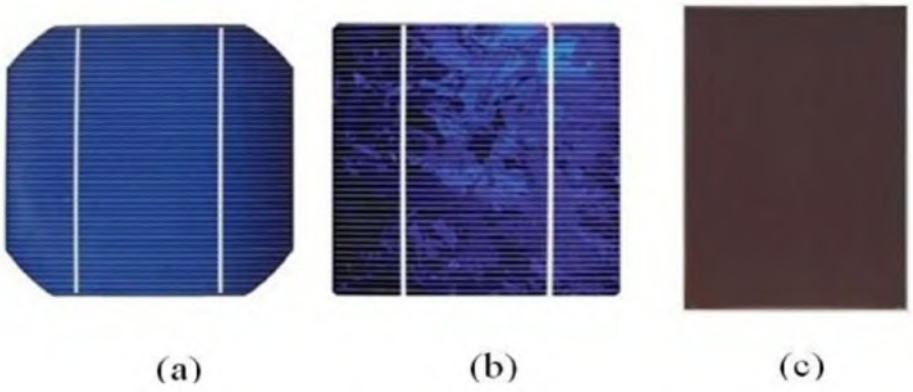

Fig I.5: Different Types of Cells

- **Monocrystalline Silicon Cell:** During cooling, the molten silicon solidifies into a single large crystal. This crystal is then sliced into thin wafers that will form the cells. These cells are typically a uniform blue color.
- **Polycrystalline Silicon Cell:** Polycrystalline cells are made up of a conglomerate of crystals. They also come from sawing crystal blocks, but these blocks are cast and thus heterogeneous. Their efficiency ranges from 13% to 20% in the laboratory [5].
- **Amorphous Silicon Cell:** Amorphous silicon cells differ from the previously mentioned cells because their structure has a high degree of disorder in the atomic arrangement [6] t. The use of amorphous silicon for solar cells has shown great advantages.

I.5 Photovoltaic Solar Energy

The sun is an inexhaustible source of energy, and the radiation reaching the Earth's surface is approximately 8400 times the annual energy consumption. This corresponds to an instantaneous peak power of 1 kW per square meter, spread across the entire spectrum, from ultraviolet to infrared. Photovoltaic solar energy involves producing electricity directly from light using solar panels. The energy comes from photons (components of light) that collide and release electrons, creating an electric current. This direct current can be converted from a small calculated power in watts peak (Wc) to alternating current through an inverter [9].

The electricity produced is available in the form of direct electricity, stored in batteries (decentralized electrical energy), or injected into the grid. The photovoltaic solar generator consists of photovoltaic modules made up of photovoltaic cells connected together.

I.6 Components of a Photovoltaic (PV) Module

A photovoltaic (PV) module is an integrated system made up of several essential components that work together to convert solar energy into electrical energy through the photovoltaic effect. Here are the key components that make up the PV module [8].

1. **Photovoltaic Cells:** These are the core components that convert sunlight into electricity using the photovoltaic effect. Photovoltaic cells are typically made from silicon, which is one of the best semiconductor materials used in this technology.
2. **Encapsulation:** This involves encapsulating the photovoltaic cells using special materials like **EVA** (Ethylene Vinyl Acetate) to protect the cells from environmental conditions such as humidity and dirt, while also providing electrical insulation.
3. **Glass:** Glass is used to protect the photovoltaic cells from external factors like wind and rain. At the same time, it allows the necessary light to pass through to generate electricity without impacting the efficiency of the cells.
4. **Frame:** The frame of the unit is typically made of aluminum. This frame serves to secure the photovoltaic cells in place and protect them, while also facilitating the installation of the module on various surfaces.
5. **Electrical Connections (Junction Boxes and Wiring):** These components allow for the connection of photovoltaic cells to one another and facilitate the transfer of the generated electricity to the external electrical system. The connections also include electrical conductors and protection against overcurrent.
6. **Backsheet:** The backsheet is attached to the rear of the PV module, usually made from polymer materials such as **Tedlar** or **Mylar**. These sheets protect the cells from environmental effects such as moisture and direct sunlight.

7. **Lamination:** The photovoltaic cells are laminated between layers of durable materials such as glass or plastic, ensuring the cells remain stable and secure over time.

These components work in harmony to effectively and efficiently convert solar energy into electricity, contributing to a reliable and sustainable energy source.

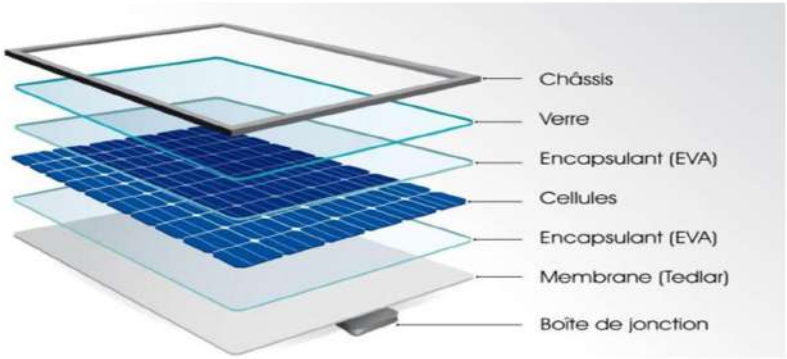

Fig I.6: Components of a Photovoltaic (PV) Module.

I.7. Components of a Solar Power System

Solar energy relies on several key components to implement and convert solar power into electricity. If you are referring to a **solar power system** (or **photovoltaic solar system**), here are the main components of such a system:

I.7.1. Solar Panels (Photovoltaic Panels)

Solar panels are the primary component for converting solar light into electricity using photovoltaic cells. The panels consist of a collection of photovoltaic cells (Photovoltaic Cells) that are grouped together.

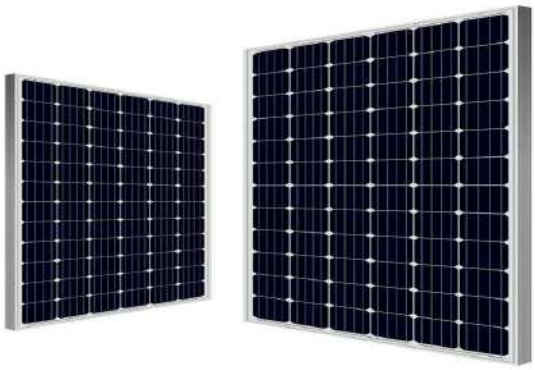

Fig I.7: Solar Panels (Photovoltaic Panels)

I.7.2. Inverter

The inverter converts the direct current (DC) generated by the solar panels into alternating current (AC), which can be used by household or commercial electrical devices. This process is essential because most devices use AC.

Fig I.8: Inverter.

I.7.3. Charge Controller

The charge controller is used to manage the charging of batteries in solar systems that store energy. It helps prevent overcharging or complete discharge of batteries, thus extending their lifespan.

Fig I.9: Charge Controller

I.7.4. Batteries

In solar systems that require energy storage, batteries are used to store the electricity generated during the day for use at night or during cloudy periods. Batteries can be of different types, such as lithium or lead-acid batteries.

Fig I.10: Batteries

I.7.5. Mounting System

This is the structure upon which the solar panels are installed. It is designed to provide stability for the panels and varies between flat roof, sloped roof, or ground installations.

Fig I.11: Mounting System

I.7.6. Wiring and Cables

Wires and cables are used to connect the solar panels to the inverter, charge controller, and batteries. The system requires wiring to safely and effectively transport current between components.

Fig I.12: Wiring and Cables

I.7.7. Energy Meter

The energy meter is used to measure the amount of electricity generated by the solar panels. It may be part of a grid-connected system to track the amount of energy produced.

Fig I.13: Energy Meter

I.7.8. Grid-Tied Inverter

In grid-connected systems, the grid-tied inverter connects the system to the public electricity grid. It allows you to send excess electricity generated by the solar panels to the grid for compensation.

Fig I.14: Grid-Tied Inverter

I.7.9. Safety Systems

These systems include fuses (circuit breakers), overcurrent protection devices, and isolation shutdown systems to ensure the safe operation of the system.

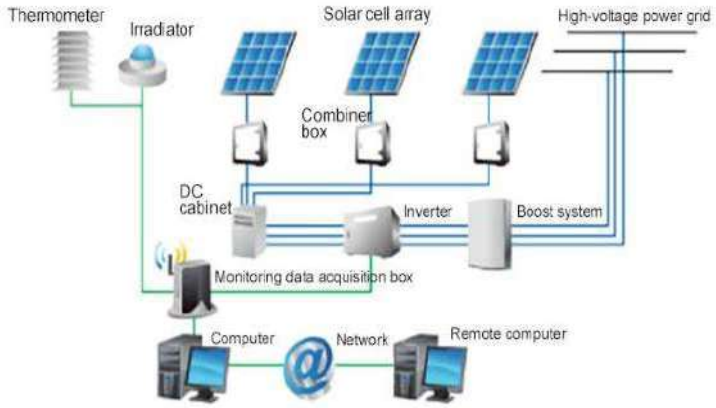

Fig I.15: Safety Systems

I.8. Connecting of photovoltaic cells

I.8.1. Connecting in series

Series connected solar cells have the same current flowing through them as they all are in the same path for current to flow. Solar PV Panels consists of multiple solar cells which are connected together in series and are enclosed in a weather proof casing. This arrangement results in a single Solar PV Panel with higher voltage output as compared to a single Solar Cell as shown in the figure below.

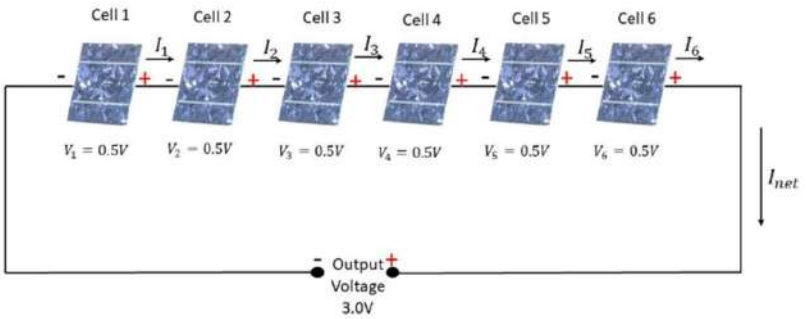

Fig I.16: Connecting of PV cells in Series.

I-8-2. Connecting in parallel

Parallel Connected Solar Cells have the same voltage across all the cells in the circuit as the terminals of one cell is connected respectively to the terminals of the other cells.

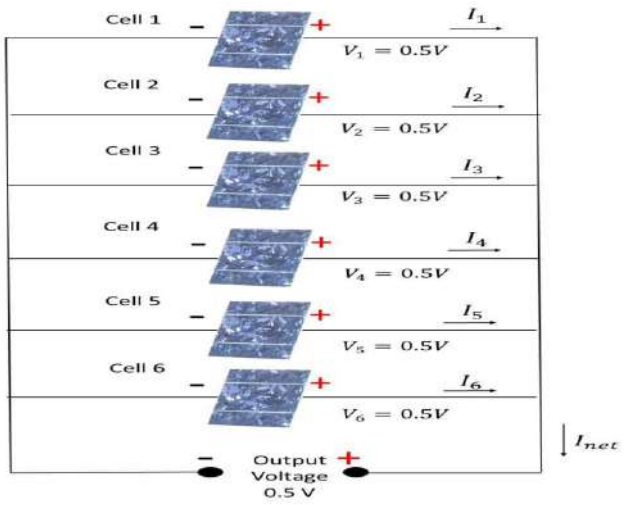

Fig I.18: Connecting of PV cells in Parallel**.**

I.9. Different Kinds of Solar Photovoltaic Systems

There are basically three types of solar power systems through which electricity can be generated. These include:

I.9.1. On-grid Photovoltaic System

In terms of both energy efficiency and cost, connecting a system to the grid (or a distribution center) is often the most effective solution for solar energy production. These systems consist of interconnected photovoltaic modules and one or more inverters. The inverter's role is to convert the direct current produced by the solar panels into alternating current to meet the requirements of the grid.

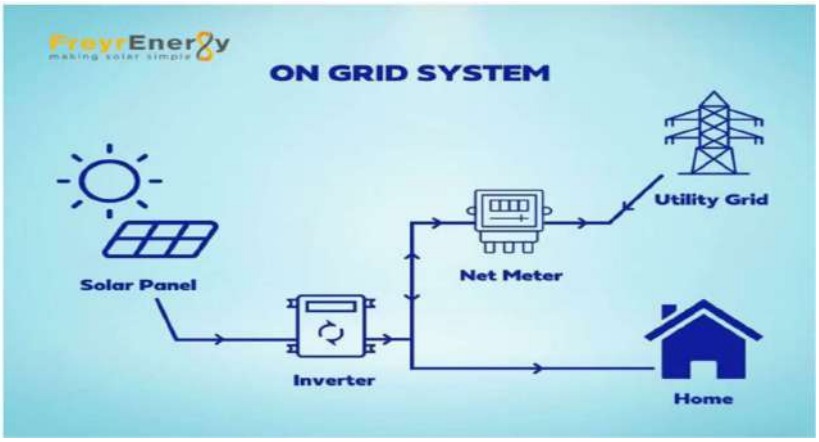

Fig I.18: On-Grid Photovoltaic System.

I.9.2. Hybrid Photovoltaic System

Hybrid systems typically involve photovoltaic setups that are paired with other energy sources, such as hybrid off-grid power plants that integrate photovoltaic fields, wind turbines, and diesel generators (backup generators). This combination allows for the consumption of renewable natural resources at production sites, ensuring a reliable supply of energy while minimizing environmental impact, regardless of weather conditions.

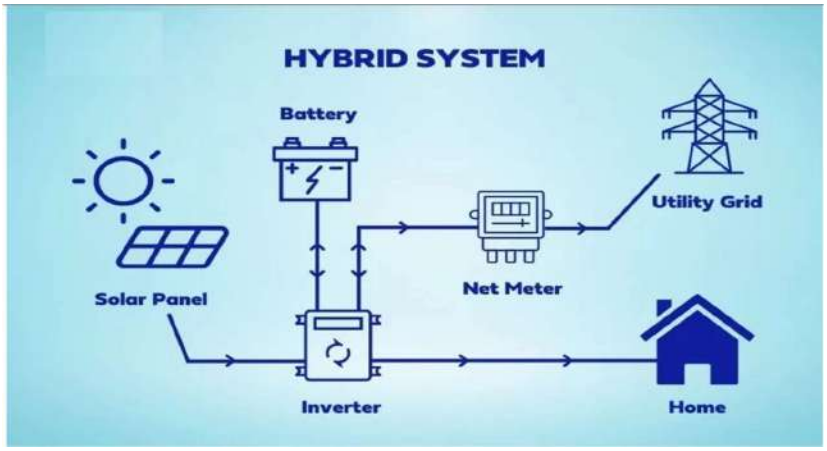

Fig I.19: Hybrid Photovoltaic System.

I.9.3. Off-grid solar

These systems are designed to operate independently without relying on external energy sources. They are commonly used in remote areas away from the grid, and depending on the application, they can be installed either without a power supply or with batteries to ensure a sufficient energy supply during extended periods of cloudy weather [9].

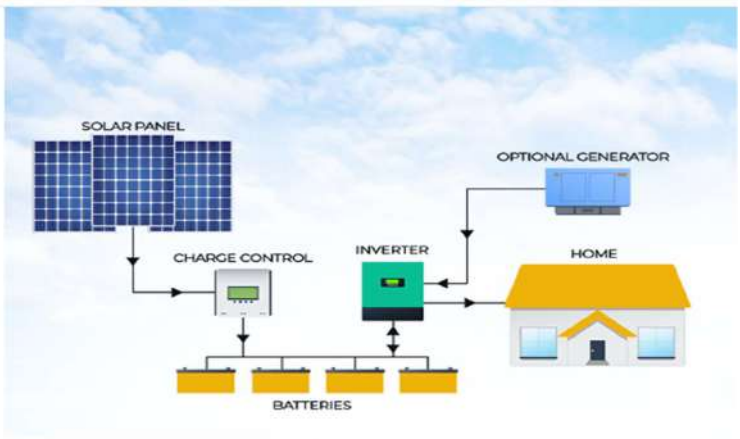

Fig I.20: Off-grid solar

I.10. Photovoltaic Pumping Systems

Many rural communities in developing countries face significant challenges due to the lack of water, with these issues being especially severe in desert regions. The water shortage in arid areas is a critical concern for local populations. Improving living conditions in these areas is closely tied

to finding effective solutions to address this problem. Photovoltaic pumping systems offer an ideal solution for water supply, especially in areas without access to an electricity grid [10].

Currently, two types of photovoltaic pumping systems are used: with batteries and without batteries. The battery-free system, while simpler, has some limitations, the main one being that its water flow depends on sunlight during the day.

I.10.1. Pumping Without Batteries

In this system, water storage is done hydraulically, with water being pumped when there is sufficient sunlight into an elevated tank. This water is then distributed by gravity as needed. The system is straightforward, with photovoltaic panels powering a pump (either surface or submerged), and a regulator controller (which may be integrated into the pump depending on the manufacturer) that ensures water is pumped when the panels are exposed to sunlight. The stored water is available for later use.

This approach is less expensive but comes with the drawback of an inconsistent flow rate, as the pump's performance depends on the sunlight available. The system does not operate during periods of low illumination (such as early morning or late afternoon), and its efficiency decreases when operating outside of its optimal power range [11].

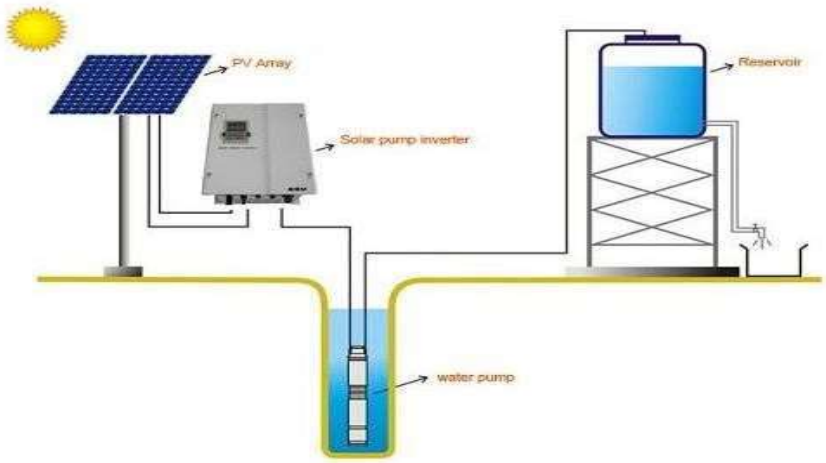

Fig I.21: Pumping without batteries.

I.10.2. Pumping with Electrochemical Storage (Batteries)

In many cases, photovoltaic pumping does not align with the required energy demand during hours of sunlight, necessitating energy storage. Using batteries in photovoltaic pumping systems ensures energy autonomy and provides a steady flow of water according to demand [12].

The batteries store electricity, which can be released when needed. To protect the batteries from damage caused by overcharging or deep discharge, a regulator is required to maintain the batteries' health and prolong their lifespan.

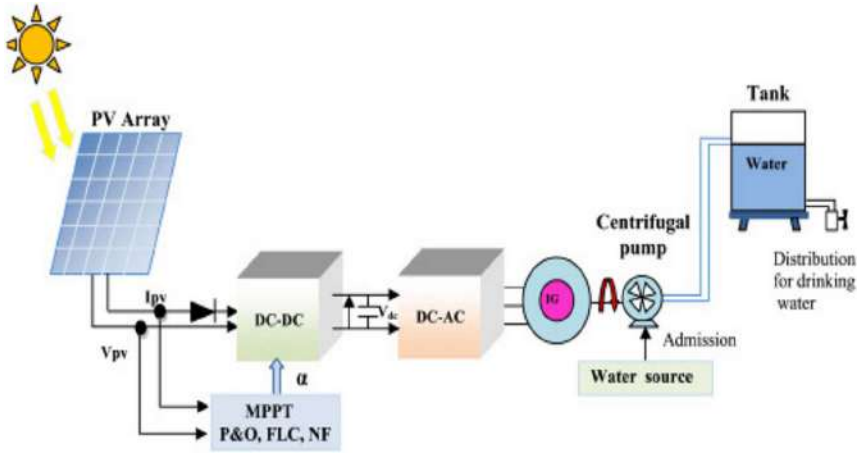

Fig I.22: Pumping with electrochemical storage.

I. 11. Components of a Photovoltaic Water Pumping System

A photovoltaic water pumping system typically consists of the following components:

1. PV generator
2. DC/DC Converter (boost)
3. DC/AC Converter (inverter)
4. Motor-pump unit

The efficiency of a solar water pumping system depends on both site-specific factors (such as sunlight, temperature, and geographical location) and equipment-related elements (including efficiency and service life). In this study, the photovoltaic pumping system includes the components shown in Fig I.23.

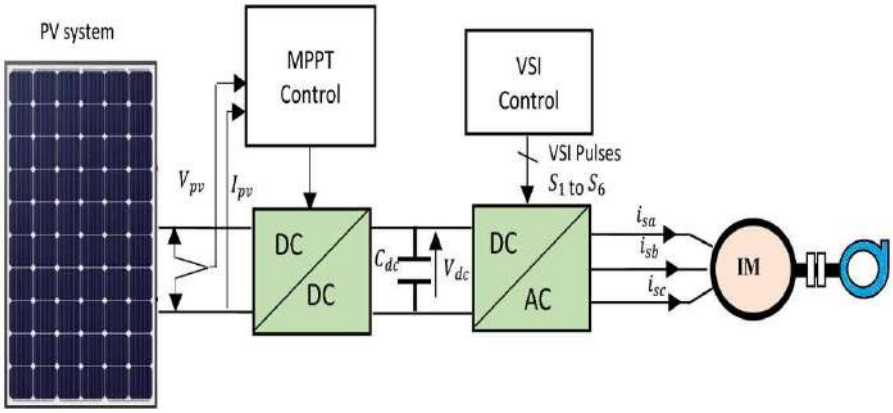

Fig I.23: PV array water pumping system design.

Photovoltaic solar panels are used to convert solar radiation into electrical energy, and these panels are electrically connected to form a direct current production unit. A power control and monitoring unit, which includes a boost converter and an inverter, is responsible for providing voltage with adjustable amplitudes and frequencies based on the available power from the solar generator. A

submerged electric pump unit, composed of an asynchronous motor and a centrifugal pump, is utilized for the pumping process.

The system also includes electrical wiring to transmit energy from the generator to the motor, as well as to handle safety control information. Additionally, there is a hydraulic infrastructure that directs the water from the well to the distribution points.

I. 11.1. PV Generator

A photovoltaic generator is made up of multiple modules, each consisting of several photovoltaic cells connected both in series and parallel to deliver the required current and voltage. The generator's performance is influenced by the variations in the modules it includes and the cells within those modules. The output voltage of the photovoltaic generator is determined by the number of modules connected in series, while the output current depends on the number of modules connected in parallel. The complete assembly of photovoltaic modules is referred to as a photovoltaic array, as illustrated in Fig (I.24).

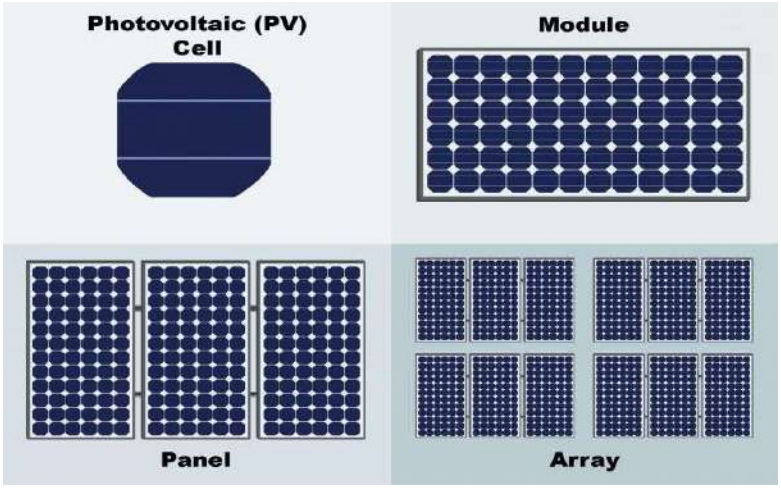

Fig .I.24**:** PV Generator**.**

I.11.2. DC-DC Converter (Chopper)

This is a direct-current to direct-current converter that uses one or more controlled switches and allows modifying the voltage of a DC source with high efficiency [16].

A parallel chopper is used when we want to increase the available voltage of a DC source (such as panels or batteries). Its start-up and shutdown control is based on a controlled switch (IGBT, MOSFET, Bipolar transistor, etc.).

A series chopper is used when the output voltage is lower than the input voltage (such as in panels or batteries). Its structure requires a controlled start-up and shutdown switch (bipolar transistor, IGBT, etc.) and a freewheeling diode. [16]

I.1.3. DC/AC Converter (Inverter)

The main function of an inverter is to convert the direct current produced by the solar generator into single-phase or three-phase alternating current. It is typically designed to operate within a fairly narrow range. It is very efficient for fixed input and output characteristics. There are countless types of DC/AC inverters depending on the quality of the output signal.

- Modified sine wave inverter.
- Pulse width modulation (PWM) inverter. [15]

The modified sine wave inverter can withstand high overloads, and its harmonic distortion is relatively low, meaning it introduces only minor losses due to the Joule effect, which could cause motor overheating.

The pulse width modulation (PWM) inverter uses fast electronic switches to vary the pulse width. Thanks to a filter at the output, the sine wave can be reconstructed. These relatively inexpensive inverters are very efficient, with efficiency approaching 90%-95%.

I.11.4. Motor-pump unit

In photovoltaic pumping systems, certain types of motors are frequently seen, such as DC motors (series excitation, shunt, permanent magnet, etc.) and AC motors (asynchronous, synchronous).

B. Pumps

Water pumps are classified as follows:

- **Principle of operation**: Either centrifugal or Positive displacement pump
- **Physical location of the pump:** in relation to the water being pumped, there are suction pumps and discharge pumps.

B.1. Centrifugal Pumps

Centrifugal pumps use variations in the speed of the pumped fluid combined with the centrifugal force effect to increase pressure. The kinetic energy transferred to the fluid is provided by the rotation of a wheel with blades or vanes, and part of this energy is converted into pressure through a decrease in speed.

The Characteristics of Centrifugal Pumps :

- The driving torque of the pump is practically zero at startup, and the pump can operate even with very low sunlight. However, a certain motor speed is required for the water pressure to be sufficient for operation.
- The absorbed power is well-suited to photovoltaic modules, providing good overall efficiency.

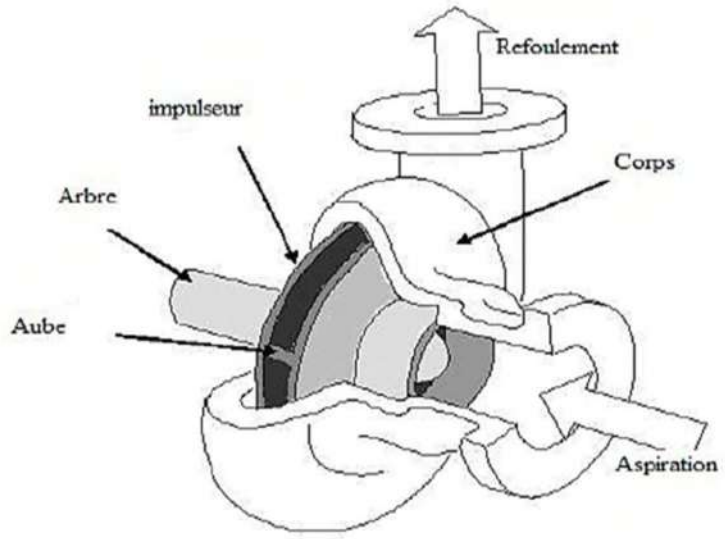

Fig I.25: Pompe centrifuge

B.2. Positive displacement pump

Positive displacement (PD) pumps are a class of pumping systems that move fluid by trapping a fixed volume and mechanically forcing it through the discharge pipe. Unlike centrifugal pumps, which rely on kinetic energy, PD pumps operate via cyclic sealing and displacement mechanisms, making them highly effective for applications requiring precise flow control or handling viscous fluids.

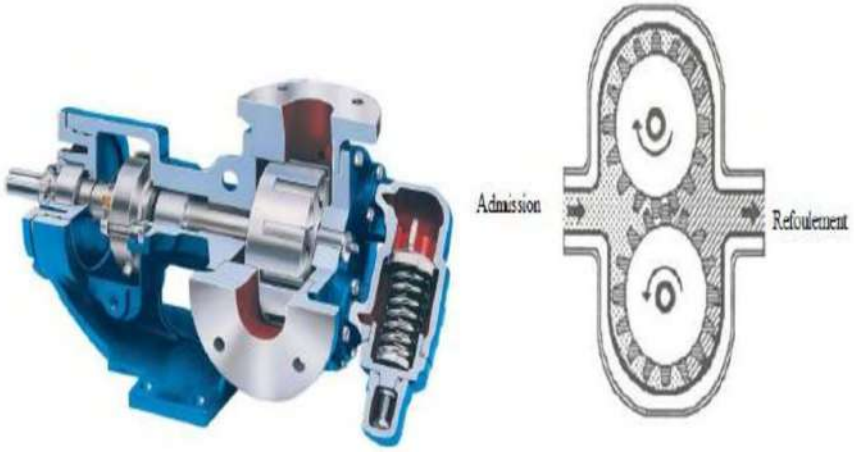

Fig. I.26: Positive displacement pump.

I.13. Advantages and disadvantages of photovoltaic systems

I.13.1 Advantages

- ✓ First, they have high reliability. The system has no moving parts, making it particularly suitable for isolated areas, which is why it is used in spacecraft.
- ✓ Operating costs are very low due to minimal maintenance, and there is no need for fuel, transportation, or specialized personnel.

- ✓ The modular nature of photovoltaic panels allows for simple assembly and adaptability to various energy needs, with systems that can be sized for power applications ranging from milliwatts to Megawatts
- ✓ Photovoltaic technology has ecological advantages since the final product is non-polluting, silent, and does not cause any environmental disturbance, except for the space occupied by large-scale installations.

I.13.2. Disadvantages

- The manufacturing of photovoltaic modules requires advanced technology and high-cost investments.
- Photovoltaic generators are not competitive with diesel generators except for low energy demands in isolated regions.
- The actual conversion efficiency of the module is low, typically in the range of 10-15%.
- They are weather-dependent.
- When electrical energy needs to be stored in chemical form (batteries), the cost of the system increases.

I.14. Conclusion

This chapter has thoroughly covered the fundamental concepts that make up a photovoltaic water pumping system. We have examined the operation of each essential component, providing a clear understanding of their individual functions. This in-depth exploration forms the foundation for the next chapter, which will focus on the modeling and analysis of these integrated systems.

Chapter II.
Modeling of the PV array and the boost converter

II.1 Introduction

Photovoltaic (PV) systems represent a promising and environmentally friendly solution for sustainable energy generation, as they convert solar energy directly into electricity via the photovoltaic effect. To optimize the efficiency and overall performance of such systems, it is essential to develop accurate mathematical models of both the PV panels and the associated DC-DC power converters. Mathematical modeling plays a fundamental role in the early design stages of photovoltaic water pumping systems, serving as the foundation for subsequent processes such as system sizing, performance optimization, and simulation. The focus of this memorandum is a photovoltaic water pumping system, which primarily consists of a photovoltaic generator, power electronic converters, and a motor-pump assembly.

This chapter focuses on the mathematical modeling of a solar panel and boost converter system, incorporating a Maximum Power Point Tracking (MPPT) control strategy. The primary objective is to optimize the efficiency of the photovoltaic (PV) system by employing MPPT algorithms, specifically the Perturb and Observe (P&O) and Incremental Conductance (INC) methods, to locate the Maximum Power Point (MPP) under varying temperature and illumination conditions.

II.2 Modeling of photovoltaic cells

II.2.1 Ideal PV cell

A photovoltaic cell can be described in a simple way in figure (II.1) as an ideal current source which produces a current i_{ph} proportional to the incident light power, in parallel with a diode which corresponds to the transition area p-n of the PV cell. If a resistive load is connected to the terminals of the photovoltaic cell, the latter delivers a current i_{pv} there [27].

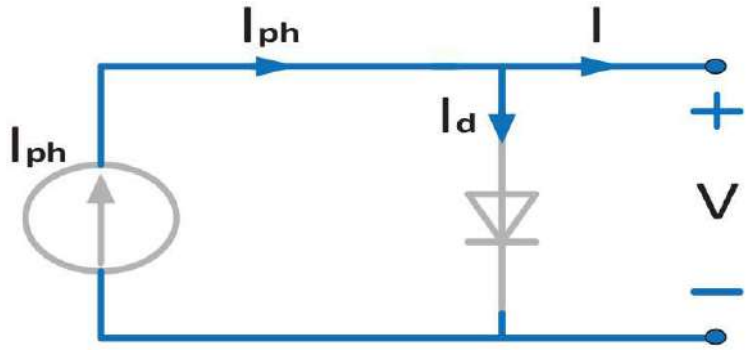

Fig II.1: Diagram of an ideal photovoltaic cell.

If the photocell is under irradiance, The current expression will be:

$$I=I_{ph}-I_d=I_{ph}-I_d\left[\exp\left(\frac{q\,V_{pv}}{a\,k_b\,T}\right)-1\right] \quad \text{(II-1)}$$

with:

I_d: the saturation current

a: the ideality factor of Junction 1<n <3

k_b: Boltzmann constant (1 ,38.10-23 J/K)

T: temperature of the cell in degrees kelvin

q: Electron charge ($1{,}602.10^{-19}$)

II.2.2 Real PV cell

The previously presented photovoltaic model does not fully capture all the physical phenomena involved in the conversion of light energy into electrical energy. In practical operation, a loss of output voltage and the presence of leakage currents are observed. To more accurately represent these effects, a series resistance R_s is introduced to model the voltage drop, while a parallel resistance R_{sh} accounts for the leakage currents within the solar cell.

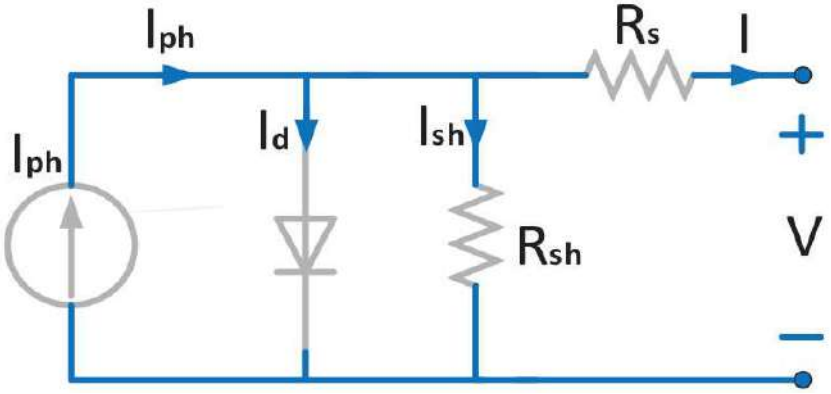

Fig II.2: Diagram of a real photovoltaic cell.

So, the expression of the cell current can have the following form:

$$I=I_{ph}-I_d-\frac{V_{pv}}{R_{sh}}=I_{ph}-I_d\left[\exp\left(\frac{q(V_{pv}+R_s\,I_{ph})}{ak_bT}\right)-1\right]-\frac{V_{pv}+R_s\,I_{ph}}{R_{sh}} \quad \text{(II-2)}$$

II.3 Modeling of a photovoltaic panels

PV cells are grouped in larger units called PV modules and these modules are connected in series or parallel to create PV arrays which are used to generate electricity in PV generation systems. The equivalent circuit for PV array is shown in Fig. 3.

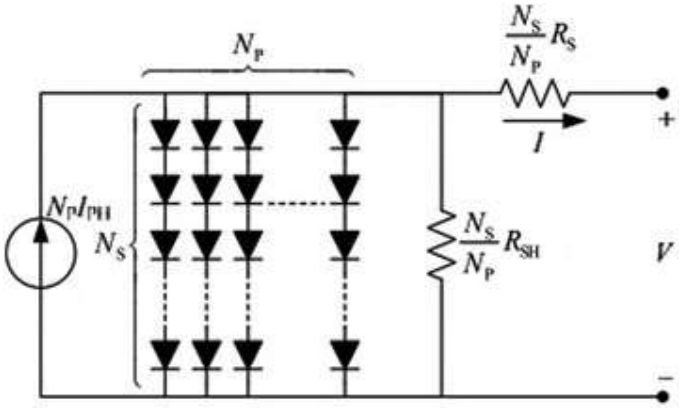

Fig II.2: Equivalent circuit of solar array

Since the association of the serial and parallel PV panels gives a PV array, its produced output current is calculated by the following expression:

$$I=n_p.I_{ph}-n_p.I_d\left[\exp\frac{1}{V_t}\left(\frac{V}{n_s}+\frac{R_s I}{n_p}\right)-1\right]-\frac{n_p}{R_{sh}}\left(\frac{V}{n_s}+\frac{R_s I}{n_p}\right) \quad \text{(II-3)}$$

with:

V_t is the array thermal voltage given by:

$$V_t=\frac{a\cdot k_b\cdot T}{q} \quad \text{(II-4)}$$

II.4 Characteristic of a photovoltaic panel

In this study, the T5-SER-235P solar module, manufactured by SunPower, is selected for analysis. The module's performance is evaluated under Standard Test Conditions **(**STC**)**, which include an irradiance of 1000 W/m² and an ambient temperature of 25°C. The electrical and operational characteristics of the module under these conditions are taken into consideration to ensure accurate modeling and performance assessment.

Table II.1: **T5-SER-235P** module from SunPower.

Parameters of the PV cell		
Maximum power (P_{mpp})[W]	**235**	**2115**
Maximum current (I_{mpp})[A]	**7.99**	**7.99**
Maximum voltage (V_{mpp})[V]	**29.42**	**264.78**
Open circuit voltage (V_{oc})[V]	**36.96**	**332.64**
Short circuit current (I_{cc})[A]	**8.48**	**8.48**

II.4.1 Current-Voltage and Power-Voltage characteristic

The characteristic of the photovoltaic **one module** in the form of Fig (II.4) and Fig (II.5).

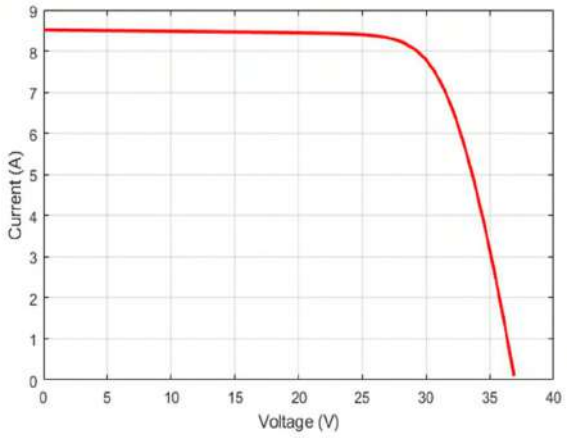

Fig II.4: Current-voltage characteristic of PV

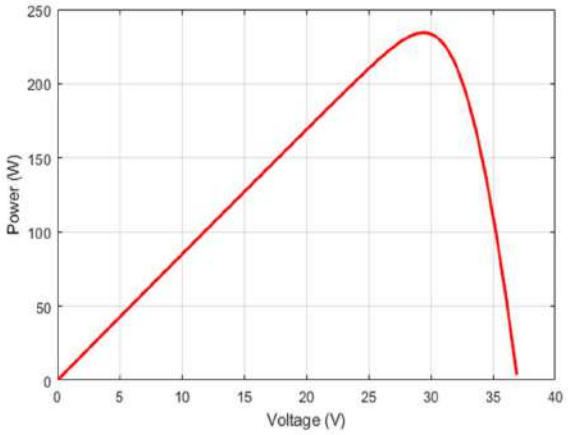

Fig II.5: Power-voltage characteristic of PV

The characteristic of the PV panels in the form of Fig II.6 and II.7

II.4.2 Influence of irradiance

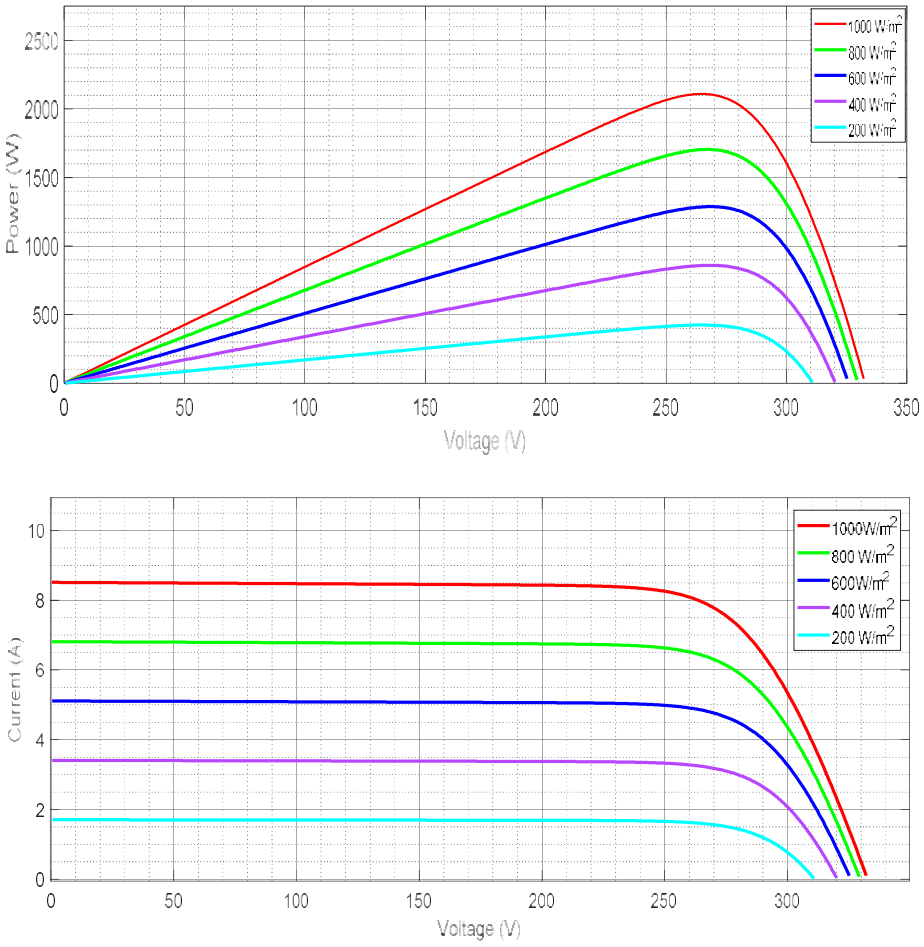

Fig II.6: The influence of irradiance on the characteristics P(V) and I(V).

The Fig (II.6) represent the Current-voltage and Power-voltage characteristics of PV modules (n_s=9 and n_p =1) at constant temperature (T=25°C.) and variable irradiance. It was observed that the value of the short-circuit current was proportional to the intensity of the radiation (luminous flux). On the other hand, the open circuit voltage does not change in the same proportion, but remains almost constant even in low irradiance.

II.4.3 Influence of temperature

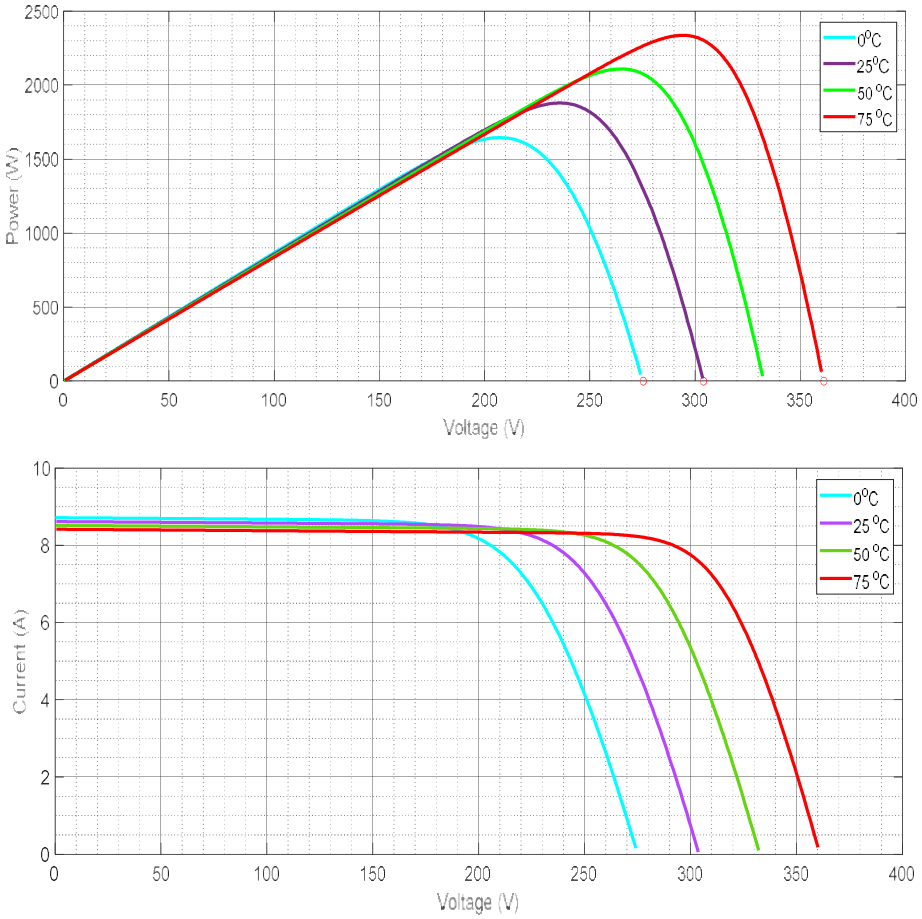

Fig II.7: The influence of temperature on the characteristics P(V) and I(V).

Fig (II.7) shows the Current-voltage and Power-voltage characteristics at a constant irradiance of 1000 W_c/h for different operating temperatures of the PV panels. It is obvious that the effect of the temperature on the value of the short-circuit current is negligible. On the other hand, when the temperature increases, the open circuit voltage decreases quite strongly.

II.5 Modeling of boost converter

Boost converter or step-up converter is a DC-to-DC converter that increases voltage. The diagram of Fig (II.8) shows the electrical circuit of the Boost.

At the first time (αT), the transistor (S) is closed, the current in the inductor gradually increases, and gradually, it stores energy, until the end of the first period. Then, the transistor (S) opens and the inductor (L) opposing the current decrease (I_L), generates a voltage which is added to the source voltage, which is applied to the load (R) through the diode (D).

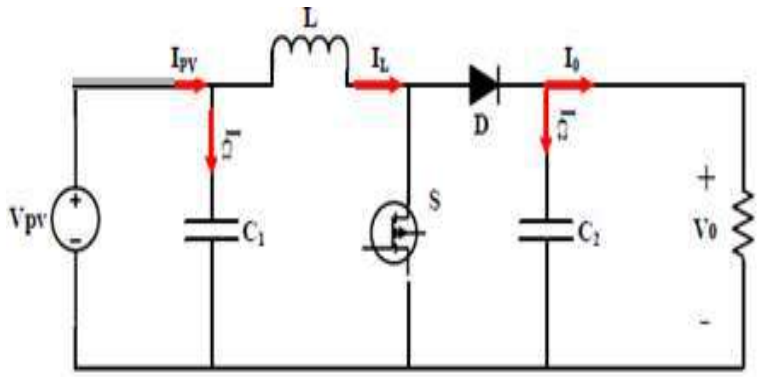

Fig II.8: Circuit diagram of Boost Converter.

II.5.1 Equivalent mathematical model

The following figures (Fig II.9) and (Fig II.10) represent the modeling of the closed and open Boost converters.

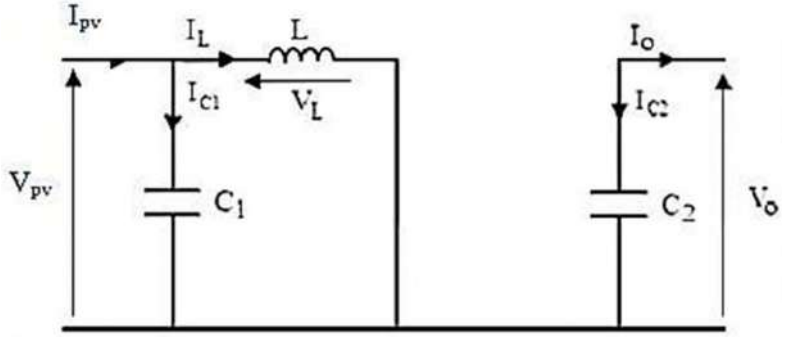

Fig II.9: Schematic diagram of a closed Boost converter.

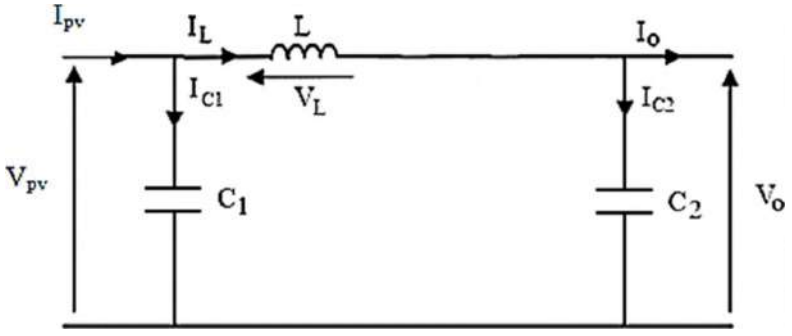

Fig II.10: Schematic diagram of an open Boost converter.

Phase 1 : $T_{On} = \alpha T\mu$

$$I_{C_1} = C_1\left(\frac{dv_{pv}}{dt}\right) = I_{pv} - I_L \qquad \text{(II-7)}$$

$$I_{C_2} = C_2\left(\frac{dv_0}{dt}\right) = -I_0 \quad \text{(II-8)}$$

$$V_L = L\left(\frac{dI_L}{dt}\right) = V_{pv} \quad \text{(II-9)}$$

Phase 2: $T_{off} = (\alpha\text{-}1)T$

$$I_{C_1} = C_1\left(\frac{dv_{pv}}{dt}\right) = I_{pv} - I_L \quad \text{(II-10)}$$

$$I_{C_2} = C_2\left(\frac{dv_0}{dt}\right) = I_L - I_0 \quad \text{(II-11)}$$

$$V_L = L\left(\frac{dI_L}{dt}\right) = V_{pv} - V_0 \quad \text{(II-12)}$$

II.6 MPPT control

The characteristics of a PV system vary with temperature and irradiation, (Fig II.6 and Fig II.7). Therefore, the MPPT algorithm must also track the newly modified maximum power point on its corresponding curve whenever variations in temperature and/or irradiation occur [27].

As we said earlier, Many MPPT algorithms are introduced in a PV system to track the maximum power point (MPP) and produce the maximum available power from a PV generator. Perturb and Observe (P&O) and Incremental conductance (IC) methods are commonly used because of the ease of implementation and simplicity.

II.6.1 Principle of the MPPT control

MPPT control is generally accomplished through DC/DC conversion circuits. The photovoltaic cell array is connected to the load through a DC/DC circuit. The maximum power tracking device continuously detects the current and voltage changes of the photovoltaic array and adjusts the PWM drive signal duty cycle of the DC/DC converter based on the changes.

For linear circuits, when the load resistance equals the source impedance, the source has maximum power output. Although photovoltaic cells and DC/DC conversion circuits are highly nonlinear, they can be considered linear circuits over a very short period of time. Therefore, by adjusting the equivalent resistance of the DC-DC conversion circuit to make it continuously equal to the internal resistance of the photovoltaic cell, the maximum output of the photovoltaic cell can be achieved, and the MPPT of the photovoltaic cell is also achieved.

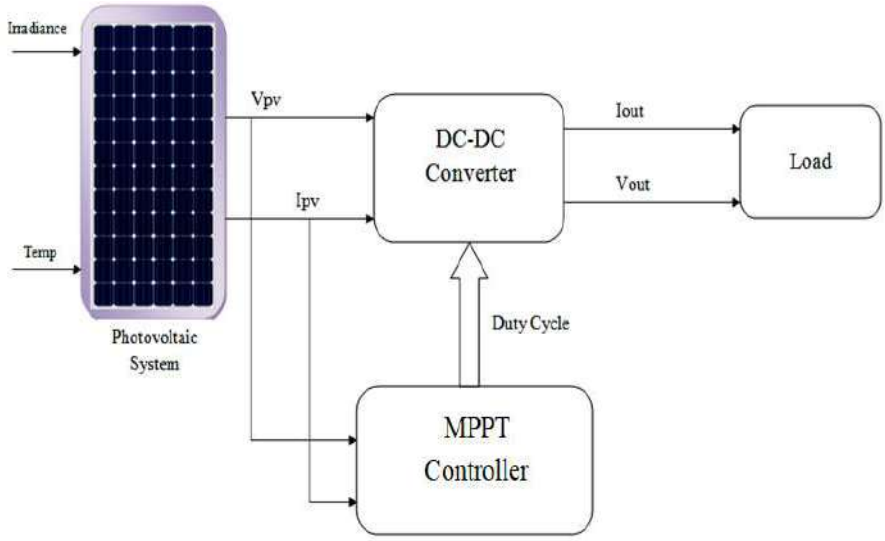

Fig II.11: Solar energy conversion chain.

II.7 MPPT Algorithms

Over the years, a wide range of Maximum Power Point Tracking (MPPT) algorithms have been developed, each offering a balance between performance such as tracking speed and accuracy and system complexity, including the need for sensors, mathematical modeling, and computational load.

Among these, the Perturb and Observe (P&O) and Incremental Conductance (INC) methods are the most commonly adopted due to their straightforward implementation and simplicity, making them suitable for practical applications.

II.7.1 Perturb and Observe (P&O) method

The principle of Perturb and Observe (P&O) type MPPT control is to perturb the PV voltage V_{PV} with a low amplitude around its initial value and analyze the behavior of the resulting power variationP_{PV}. As illustrated in Fig (II.12), one can deduce that if a positive increment in voltage V_{PV} results in an increase in power P_{PV}. it means the operating point is to the left of the MPP. Conversely, if the power decreases, it implies that the system has exceeded the MPP. Similar reasoning can be applied when the voltage decreases. Based on these analyses of the consequences of voltage variation on the P_{PV}.(V_{PV}) characteristic, it is then easy to position the operating point relative to the MPP and converge it towards maximum power through an appropriate control command. [28].

Represents the classic algorithm associated with P&O type MPPT control, where power evolution is analyzed after each voltage perturbation. For this type of control, two sensors (current and voltage of the PV generator) are required to determine the PV power at each instant. Figure II.13 represents the classic algorithm associated with P&O type MPPT control, where power evolution

is analyzed after each voltage perturbation. For this type of control, two sensors (current and voltage of the PV generator) are required to determine the PV power at each instant.

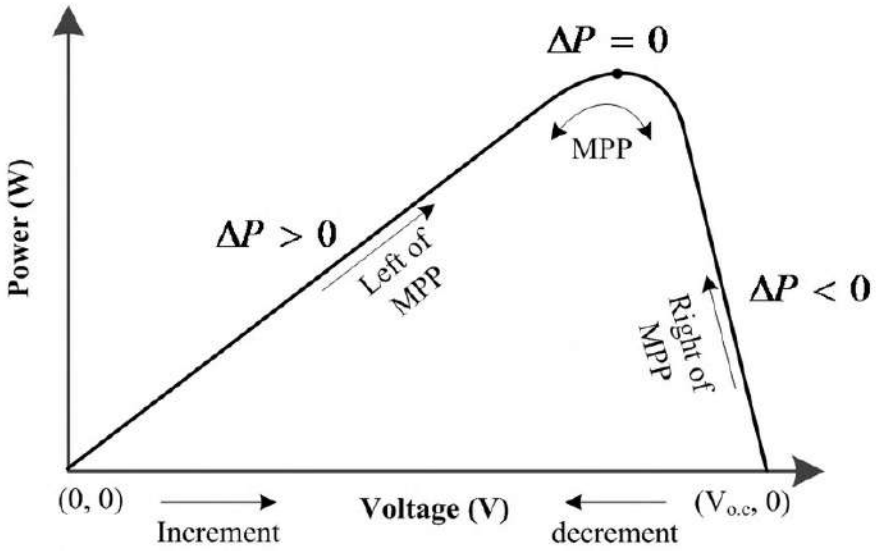

Fig II.12: Graph of Power-voltage of P&O algorithm.

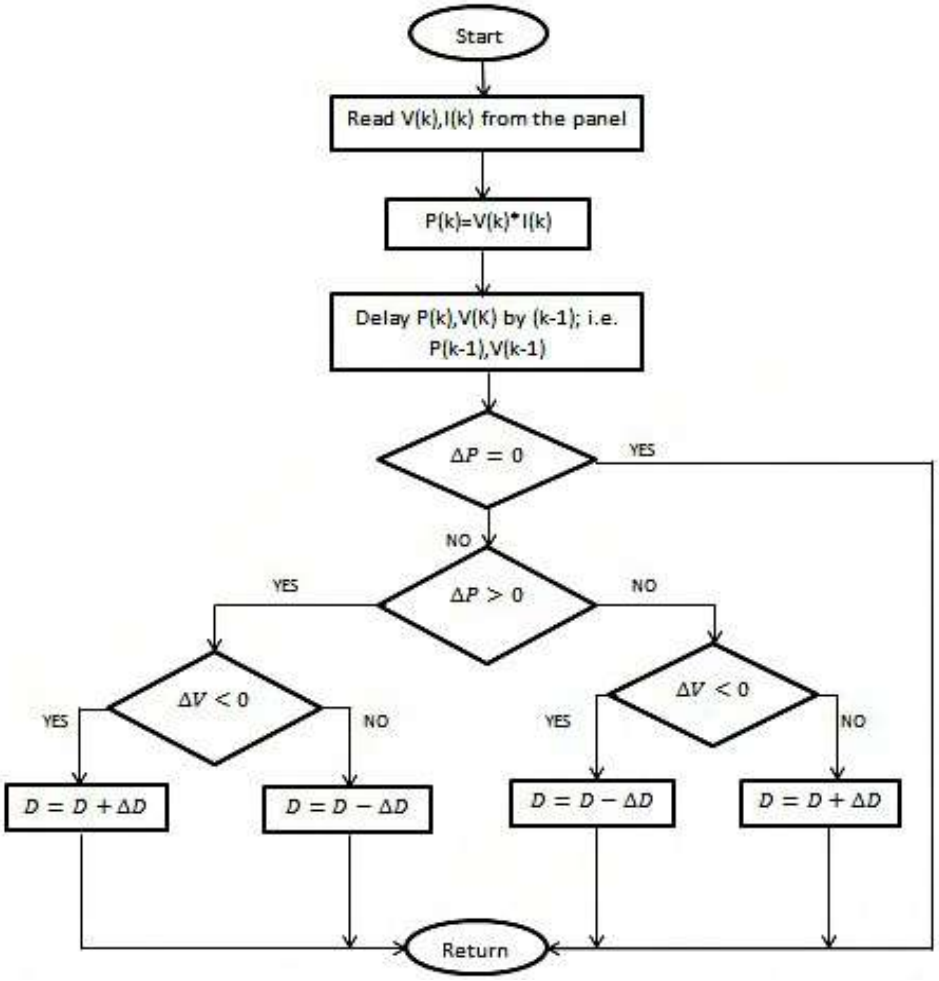

Fig II.13: Flowchart of Perturb and Observe (P&O) algorithm.

II.7.2 Incremental Conductance (INC) method

The Incremental Conductance (INC) algorithm is a widely used and well-established MPPT method. It relies on measuring both the operating voltage V and current I of the photovoltaic (PV) module using two sensors. The core principle of this technique is that the derivative of the output power P with respect to the module voltage V becomes zero at the Maximum Power Point (MPP). By continuously analyzing this relationship, the INC algorithm can accurately track and maintain operation at the MPP under varying environmental conditions.

The Incremental Conductance (INC) algorithm offers greater precision in identifying the Maximum Power Point (MPP) compared to the Perturb and Observe (P&O) method, which tends to oscillate around the MPP. The INC technique accurately tracks the MPP by comparing the incremental conductance with the instantaneous conductance of the photovoltaic (PV) array

One of the key advantages of this method is its ability to respond rapidly and accurately to dynamic changes in solar irradiance, whether increasing or decreasing. However, this enhanced accuracy comes at the cost of greater algorithmic complexity, making the INC method more demanding in terms of implementation when compared to the simpler P&O approach.

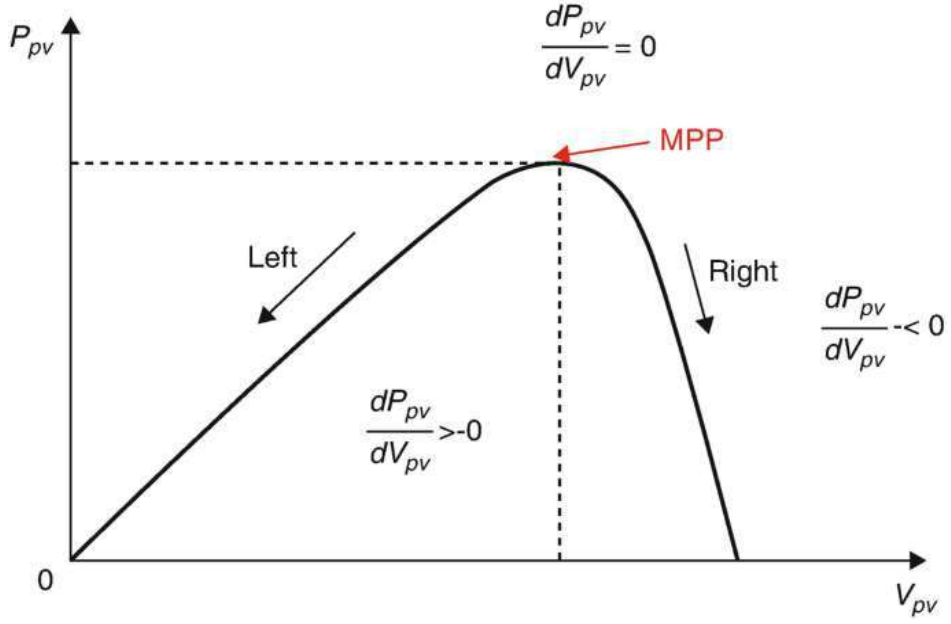

Fig II.14: Graph of power/voltage of INC algorithm.

The algorithm can be easily understood by the following flow chart which is shown in Fig (II.15).

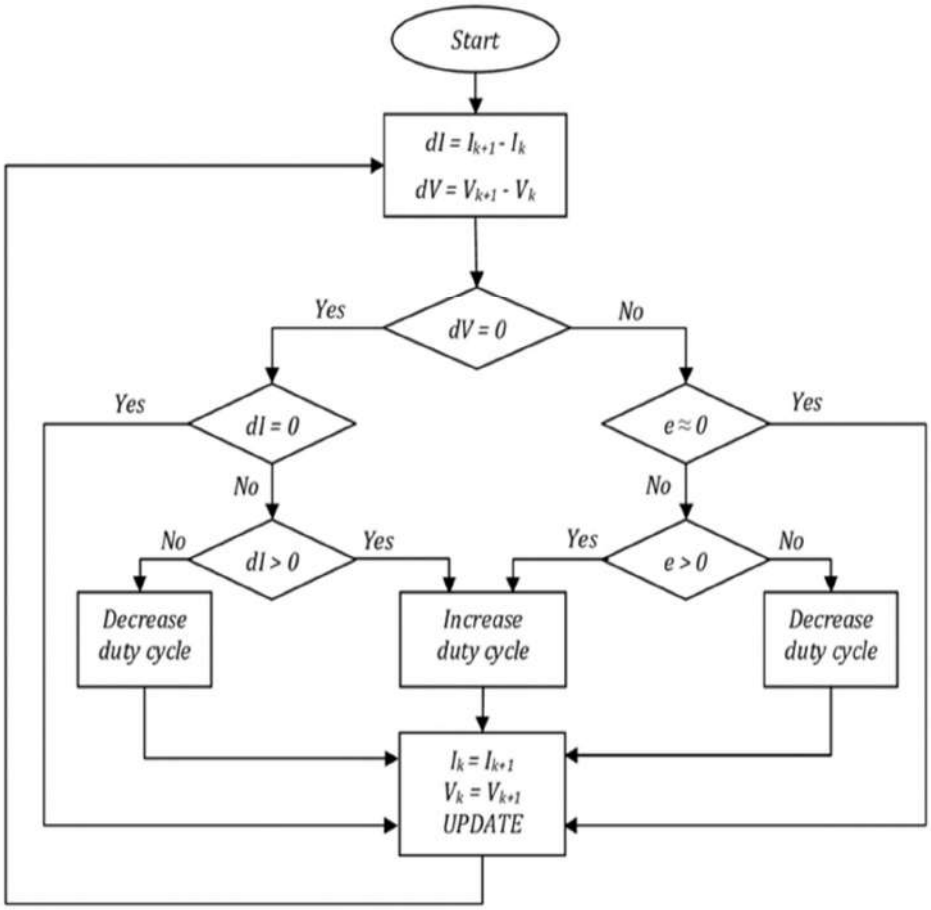

Fig II.15: Flowchart of Incremental Conductance (INC) method algorithm.

II.8 Simulation of the PV system with MPPT control

- The system is simulated under standard conditions (G=1000W/m2, T=25C) to extract the optimal power from our system.
- The electrical characteristics of the Boost converter and the Parameters of The PV cell used in this work are given in the Appendix.

II.8.1 Simulation diagram

Fig (II.16) shows the block diagram of simulation using the MATLAB/SIMULINK software of the photovoltaic system using Perturb and Observe and Incremental Conductance Methods.

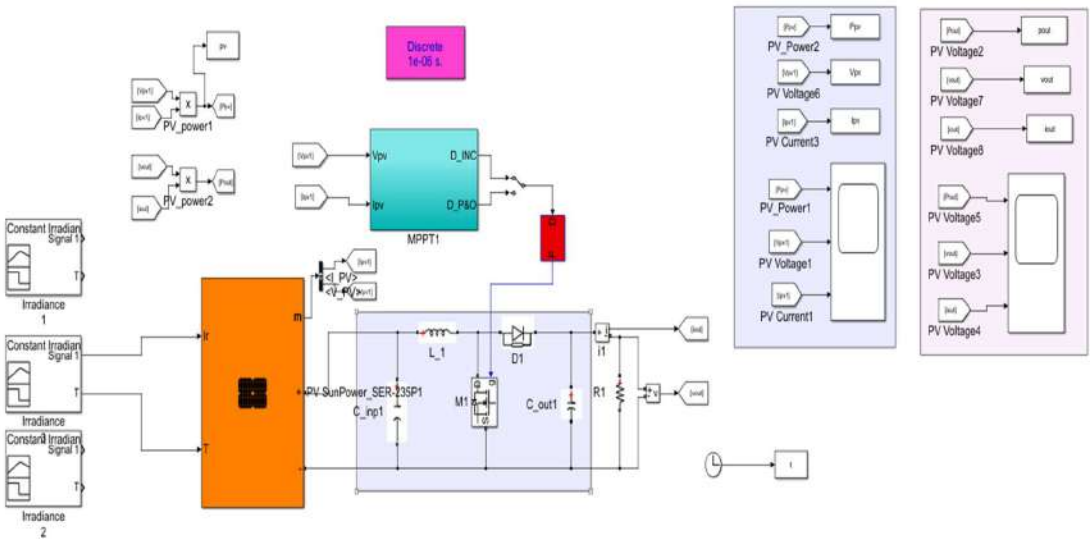

Fig II.16: Matlab/Simulink diagram of the photovoltaic system with P&O and INC Methods

II.8.2 Simulation results with Irradiance at variable (P&O and INC) Algorithm

The input results of the system, under constant temperature (25°C) and varying irradiance levels, highlight the dynamic behavior of the photovoltaic (PV) array when using the two MPPT algorithms: Perturb & Observe (P&O) **in green**, and Incremental-Conductance (INC) **in purple**. The input current reaches a peak of approximately 8 A under maximum irradiance and decreases to 6 A and then to around 5 A as irradiance drops. Both algorithms exhibit similar current trends, with INC showing slightly smoother transitions during dynamic changes. The input voltage remains relatively steady, fluctuating between 270 V and 295 V, with P&O exhibiting slightly more oscillations during transient phases.

The input power closely follows the irradiance profile, peaking near 2200 W and dipping to 1400 and 1200 W as expected. Notably, the INC method demonstrates better stability and quicker settling, especially during sudden irradiance changes.

When correlated with the output results, a clear relationship emerges: the output current, voltage, and power shown **in blue for P&O** and **red for INC** mirror the variations observed in the input. The output current starts near 4.8 A, dropping to about 3.5 A in lower irradiance intervals, and increases again as irradiance rises. The output voltage ranges from 330 to 450 V, maintaining good regulation across all conditions. The output power, much like the input, peaks around 2200 W and shows responsive tracking to the irradiance changes. The INC method continues to display superior dynamic behavior, with reduced oscillations and better stability across the output variables.

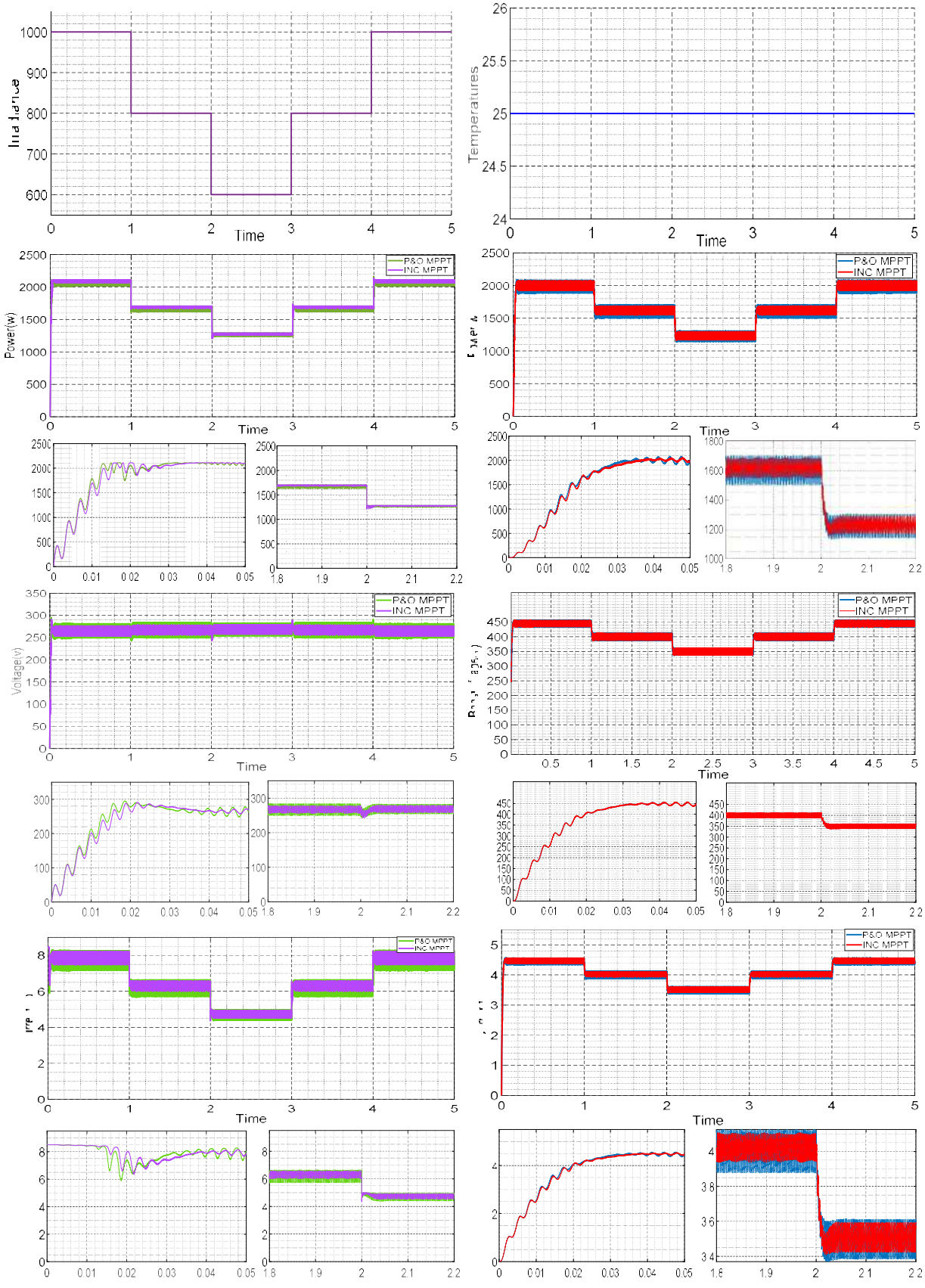

Fig II.16 Simulation results with Irradiance at variable (P&O and INC) Algorithm.

II.8.3 Simulation results with Temperature at variable (P&O and INC) Algorithm.

Under the new conditions, which involve a constant solar irradiance of 1000 W/m² and a gradual change in temperature from 25° to 35°, then to 40°C, and finally back to 25°C, the system's input behavior reveals the direct impact of temperature on photovoltaic performance.

The output current remained relatively stable around 8 A for both MPPT algorithms (P&O and INC), with the INC algorithm showing faster stabilization and reduced oscillations during transitional phases. The output voltage, however, was clearly affected by the increase in temperature, decreasing gradually as the temperature rose a known physical behavior due to the thermal properties of solar cells.

Notably, the INC algorithm (**purple line**) maintained a more stable voltage response than the P&O method (**green line**), which exhibited larger fluctuations during temperature shifts. Regarding the output power, it dropped progressively from approximately 2100 W to around 1900 W as temperature increased, reflecting the thermal efficiency losses in the system. Despite this reduction, the INC method demonstrated a more coherent and stable power output compared to P&O, highlighting its superiority in adapting to sudden thermal variations.

These results clearly underscore the effectiveness of the INC algorithm in managing dynamic environmental conditions, making it a more reliable choice for maximizing energy extraction in PV systems.

Comparing these input dynamics to the output performance further underscores the impact of environmental conditions and control strategy. The output power, shown in the first figure, mirrors the changes in irradiance decreasing from about 2000 W to 1600 W, and then increasing again while maintaining closer tracking to the maximum power point with INC (**red curve**) than with P&O (**blue curve**), especially during transients. The output current stabilized around 4.8 A but exhibited significantly fewer oscillations with INC. Similarly, the boost converter voltage output remained near 450 V, with transient dips corresponding to changes in irradiance, yet INC again showed faster and more stable convergence. These results confirm that under the same input conditions, the INC MPPT algorithm consistently provides better performance, with improved dynamic response and reduced power losses, making it the more effective strategy for maximizing energy extraction in real-world PV systems.

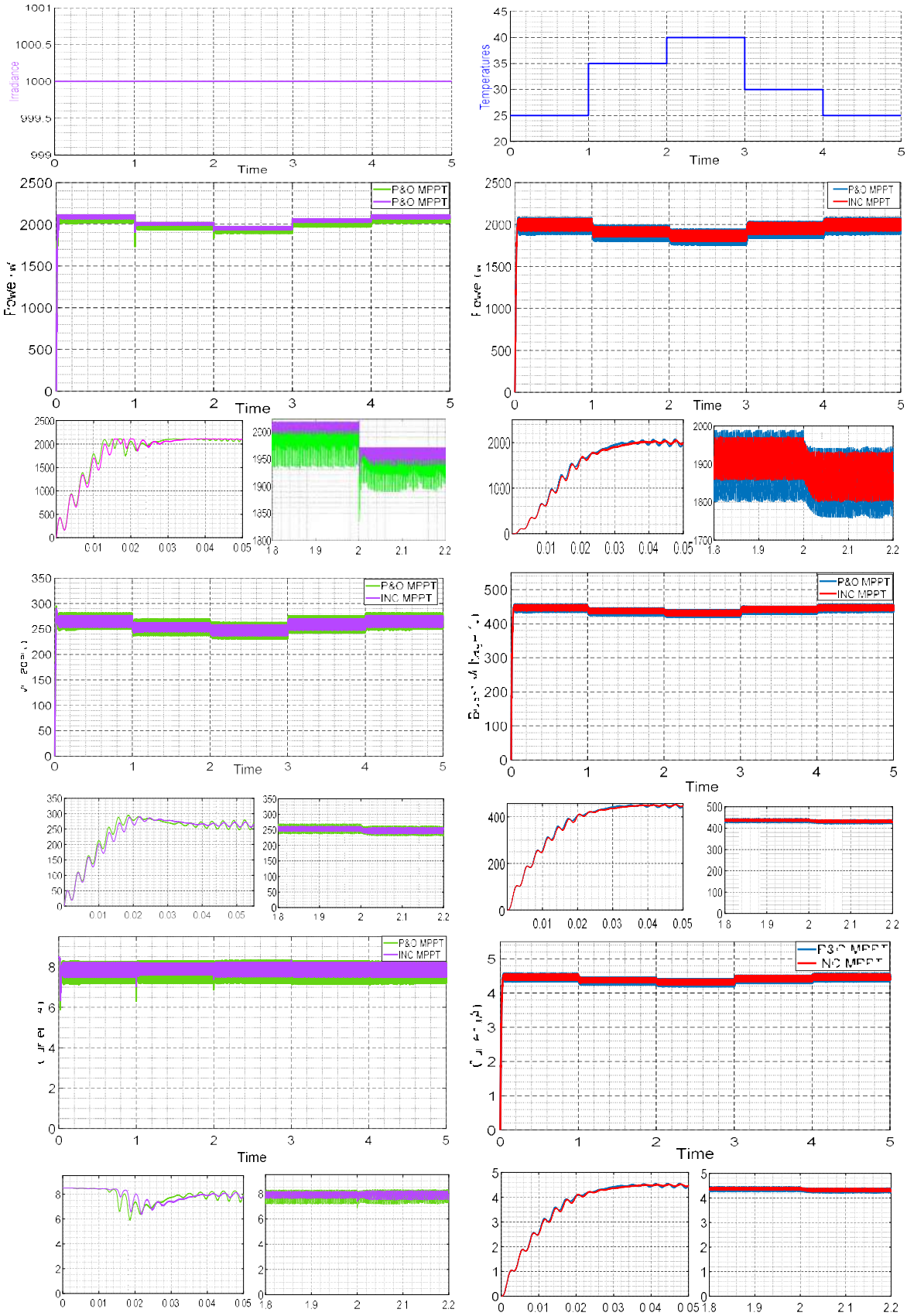

Fig II.17 Simulation results with temperature at variable (P&O and INC) Algorithm

II.8.4 Interpretation of MPPT algorithm performance

The simulation results indicate that the Perturb and Observe (P&O) method, despite its simplicity and ease of implementation, suffers from inherent perturbation-based behavior that often leads to oscillations around the Maximum Power Point (MPP). These oscillations can reduce the overall efficiency of the Maximum Power Point Tracking (MPPT) process and may introduce instability into the system.

In contrast, the Incremental Conductance (INC) method utilizes the derivative of power with respect to voltage to determine the appropriate direction toward the MPP. According to the simulation findings, this algorithm demonstrates superior accuracy in tracking the MPP compared to the P&O method. However, continuous monitoring is required to maintain optimal performance, as the INC method can also exhibit oscillatory behavior under certain conditions.

II.9 Conclusion

In this chapter, a comprehensive modeling of the photovoltaic (PV) array and the boost converter was presented, laying the foundation for effective energy conversion in solar-powered water pumping systems. The mathematical representations of both ideal and real PV cells were developed to accurately reflect the electrical behavior of solar panels under varying environmental conditions. Additionally, the boost converter was modeled and analyzed as a vital interface for voltage regulation and power optimization.

The integration of Maximum Power Point Tracking (MPPT) techniques was also examined in detail, with a particular focus on the Perturb and Observe (P&O) and Incremental Conductance (INC) algorithms. Simulation results highlighted the trade-offs between these two methods: while P&O is simple and easy to implement, it is prone to oscillations near the MPP. On the other hand, the INC method offers higher accuracy and faster adaptation to changes in irradiance, albeit at the cost of greater complexity.

Overall, the models and control strategies discussed in this chapter form the theoretical and practical basis for optimizing the performance of PV systems in dynamic operating conditions. These findings will serve as essential inputs for the subsequent implementation and validation stages of the proposed control strategy.

Chapter III.
Modeling of an induction motor, centrifugal pump and inverter

III.1 Introduction

The induction motor is among the most widely used types of electric motors in industrial applications, thanks to its low cost and high torque density. It also offers several advantages, including a simple design and high durability [30].

This chapter delves into the mathematical modeling of these essential elements: the induction motor, centrifugal pump, and inverter. By establishing a robust mathematical framework, we gain a deeper understanding of their individual characteristics and how they interact within the broader system.

III.2 Modeling of the Induction Motor

The Induction Motor is currently the most widely used electric motor in industry. Its main advantage lies in the absence of sliding electrical contacts, which leads to a simple, robust and easy to build structure, its stator is connected directly to the industrial network at constant voltage and frequency, it rotates at a speed lower than the synchronism speed; it is it that is used for the realization of almost all drives at constant speed. It also allows the realization of variable speed drives and the place it occupies in this field is constantly growing.

III.2.1 Simplifying assumptions

An induction machine, with its windings distribution and geometry, is so complex that it cannot be analyzed, taking into account its exact configuration. Then, it is necessary to adopt simplifying assumptions [34, 35]:

- The magnetic fields are supposed unsaturated.
- The skin effect does not exist.
- The machine has a constant air gap, which made the slotting effect is not taken account.
- The MMFs created by the different circuits of stator and rotor are spread to have sinusoidal repartitions.

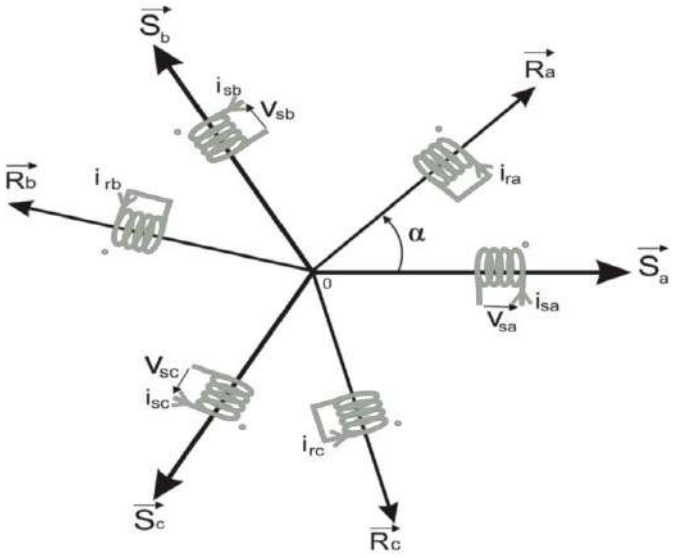

Fig III.1: Representation of the induction machine.

III.2.2 The equations the induction motor

The behavior of the induction motor is entirely defined by three types of equations:

- The electrical equations.
- The magnetic equations.
- The mechanical equations

III.2.2.1 The electrical equations

By applying the generalized ohm's law for each phase:

$$\begin{cases} V_{sabc} = [R_s] \cdot [i_{sabc}] + (d/dt) \cdot [\Phi_{sabc}] \\ V_{rabc} = [R_r] \cdot [i_{rabc}] + (d/dt) \cdot [\Phi_{rabc}] \end{cases} \quad \text{(III-1)}$$

with:

$$[R_s] = \begin{bmatrix} R_s & 0 & 0 \\ 0 & R_s & 0 \\ 0 & 0 & R_s \end{bmatrix} ; \quad [R_r] = \begin{bmatrix} R_r & 0 & 0 \\ 0 & R_r & 0 \\ 0 & 0 & R_r \end{bmatrix} \quad \text{(III-2)}$$

$$[V_{sabc}] = \begin{bmatrix} V_{sa} \\ V_{sb} \\ V_{sc} \end{bmatrix} ; \quad [V_{rabc}] = \begin{bmatrix} V_{ra} \\ V_{rb} \\ V_{rc} \end{bmatrix} \quad \text{(III-3)}$$

$$[\Phi_{sabc}] = \begin{bmatrix} \Phi_{sa} \\ \Phi_{sb} \\ \Phi_{sc} \end{bmatrix} ; \quad [\Phi_{rabc}] = \begin{bmatrix} \Phi_{ra} \\ \Phi_{rb} \\ \Phi_{rc} \end{bmatrix} \quad \text{(III-4)}$$

$$[i_{sabc}] = \begin{bmatrix} i_{sa} \\ i_{sb} \\ i_{sc} \end{bmatrix} ; \quad [i_{rabc}] = \begin{bmatrix} i_{ra} \\ i_{rb} \\ i_{rc} \end{bmatrix} \quad \text{(III-5)}$$

III.2.2.2 The magnetic equations

The relationship between the totalized fluxes on the windings and the currents can be described by the following matrix equation:

$$\begin{bmatrix} \Phi_{sabc} \\ \Phi_{rabc} \end{bmatrix} = \begin{bmatrix} [L_{ss}] & [M_{sr}] \\ [M_{rs}] & [L_{rr}] \end{bmatrix} . \begin{bmatrix} i_{sabc} \\ i_{rabc} \end{bmatrix} \quad \text{(III-6)}$$

So:

$$[\Phi_{sabc}] = [L_{ss}] \cdot [i_{sabc}] + [M_{sr}] \cdot [i_{rabc}] \quad \text{(III-7)}$$

$$[\Phi_{rabc}] = [L_{rr}] \cdot [i_{rabc}] + [M_{rs}] \cdot [i_{sabc}] \quad \text{(III-8)}$$

With: Φ_s : stator flux ; Φ_r : rotor flux

$$[L_{ss}] = \begin{bmatrix} l_s & M_s & M_s \\ M_s & l_s & M_s \\ M_s & M_s & l_s \end{bmatrix}; \qquad [L_{rr}] = \begin{bmatrix} l_r & M_r & M_r \\ M_r & l_r & M_r \\ M_r & M_r & l_r \end{bmatrix} \quad \text{(III-9)}$$

$$[M_{sr}] = [M_{rs}]^t = M'_{sr} \begin{bmatrix} \cos(\alpha) & \cos(\alpha+2\pi/3) & \cos(\alpha-2\pi/3) \\ \cos(\alpha-2\pi/3) & \cos(\alpha) & \cos(\alpha+2\pi/3) \\ \cos(\alpha+2\pi/3) & \cos(\alpha-2\pi/3) & \cos(\alpha) \end{bmatrix} \quad \text{(III-10)}$$

Finally, there exists:

$$\begin{cases} [V_{sabc}] = [R_s][i_{sabc}] + (d/dt) \cdot ([L_{ss}] \cdot [i_{sabc}] + [M_{sr}] \cdot [i_{rabc}]) \\ [V_{rabc}] = [R_r][i_{rabc}] + (d/dt) \cdot ([L_{rr}] \cdot [i_{rabc}] + [M_{rs}] \cdot [i_{sabc}]) \end{cases} \quad \text{(III-11)}$$

III.2.2.3 The mechanical equations

To study electromechanical transient phenomena with a variable rotor speed (for example starting, braking, variation of the load on the shaft, etc ....), it is necessary to add the equation of motion to the system of differential equations.

$$J . \frac{d\Omega_r}{dt} = T_{em} - T_r - f . \Omega_r \quad \text{(III-12)}$$

with :

T_{em}: electromagnetic torque.

T_r: resistant torque that can be a function of speed.

J: moment of inertia of the rotating masses.

f: viscous friction coefficient.

Ω_r : Speed of rotation of the machine.

III.3 Park's transformation

In order to reduce the expressions of the induction motor equation given below and obtain constant coefficients in the differential equations, the Park's transform will be applied. Especially, it can understand as transforming the three windings of the induction motor to jest two windings, as shown in Figure III.2.

In the context of electrical machines, the d-q reference frame simplifies modeling. By using the Park transformation, we can express the behavior of the machine in terms of two inductors (d and q) instead of three fixed real inductors. This approach streamlines the analysis while making certain assumptions about the system.

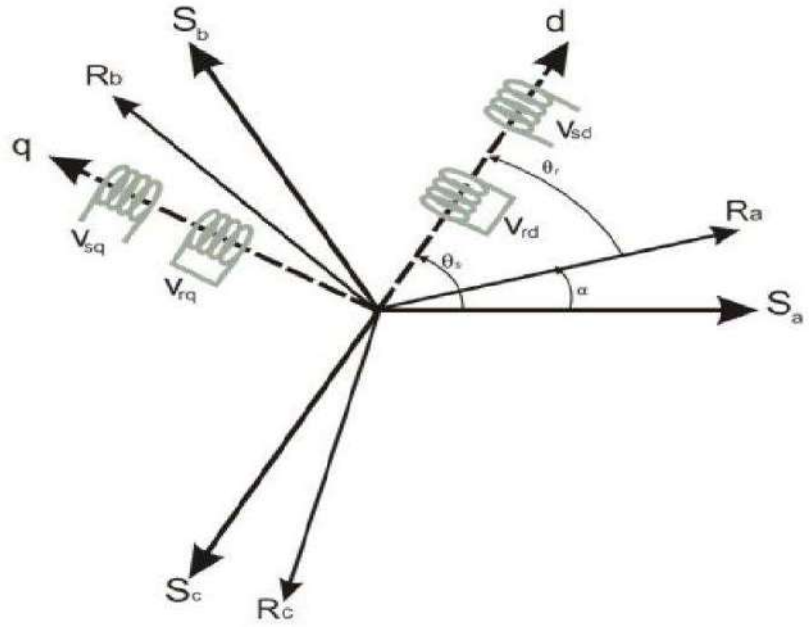

Fig III.2: Principle of Park's Transformation (Three-phase to Two-phase).

The Park transformation's representation, in general, is given as:

$$\left[P(\theta)\right]=\sqrt{\frac{2}{3}}\cdot\begin{bmatrix}\cos(\theta) & \cos\left(\theta-\frac{2\pi}{3}\right) & \cos\left(\theta-\frac{4\pi}{3}\right)\\ -\sin(\theta) & -\sin\left(\theta-\frac{2\pi}{3}\right) & -\sin\left(\theta-\frac{4\pi}{3}\right)\\ \frac{1}{\sqrt{2}} & \frac{1}{\sqrt{2}} & \frac{1}{\sqrt{2}}\end{bmatrix} \quad \text{(III-13)}$$

$$\begin{bmatrix}x_d\\ x_q\\ x_0\end{bmatrix}=P(\theta)\cdot\begin{bmatrix}x_a\\ x_b\\ x_c\end{bmatrix} \quad \text{(III-14)}$$

III.3.1 Application of the Park transformation

The expressions of the machine (III-1) can be expressed using the passage matrix is that considering that the system is balanced:

III.3.1.1 The electrical equations

$$\begin{cases} V_{sd} = R_s i_{sd} + \dfrac{d}{dt}\Phi_{sd} - \omega_a \Phi_{sq} \\ V_{sq} = R_s i_{sq} + \dfrac{d}{dt}\Phi_{sq} + \omega_a \Phi_{sd} \\ V_{rd} = 0 = R_r i_{rd} + \dfrac{d}{dt}\Phi_{rd} - (\omega_a - \omega_r)\Phi_{rq} \\ V_{rq} = 0 = R_r i_{rq} + \dfrac{d}{dt}\Phi_{rq} + (\omega_a - \omega_r)\Phi_{rd} \end{cases} \quad \text{(III-15)}$$

III.3.1.2 The magnetic equations

$$\begin{cases} \Phi_{sd} = L_s \cdot i_{sd} + M \cdot i_{rd} \\ \Phi_{sq} = L_s \cdot i_{sq} + M \cdot i_{rq} \\ \Phi_{rd} = L_r \cdot i_{rd} + M \cdot i_{sd} \\ \Phi_{rq} = L_r \cdot i_{rq} + M \cdot i_{sq} \end{cases} \quad \text{(III-16)}$$

$L_s = l_s - m_s$: the cyclic inductance of the stator

$L_r = l_r - m_r$: the cyclic inductance of the rotor.

$M = \dfrac{3}{2} M_{sr}$: the mutual cyclic inductance between stator and rotor.

III.3.1.3 The mechanical equations

The application of the Park transformation for the mechanical equation gives:

$$T_{em} = p\left(\Phi_{rd} i_{sq} - \Phi_{rq} i_{sd}\right) \quad \text{(III-17)}$$

The equation of motion of the machine is then written:

$$J.\frac{d\Omega_r}{dt} = T_{em} - T_r - f.\Omega_r \quad \text{(III-18)}$$

III.4 Model of the induction motor

In a three-phase induction motor powered by a voltage source, the stator voltages (V_{alpha_s} and V_{bata_s}) and the rotating field speed (ω_r) serve as the primary control variables. Conversely, the resistance torque (T_r) acts as an external disturbance that can disrupt the system's behavior.

To express the machine model as an equation of state, the equations need modification to represent them as a function of the state vector variables X_u. Following simplification and rearrangement, the resulting expression is:

$$X_u^{\bullet} = A_u \cdot X_u + B_u U \tag{III-19}$$

With:

$$A=\begin{bmatrix} 0 & \omega_{dq} & -R_s & 0 \\ -\omega_{dq} & 0 & 0 & -R_s \\ \frac{1}{\sigma L s T_r} & \frac{1}{\sigma L_s}\omega_r & -\frac{1}{\sigma T_s}-\frac{1}{\sigma T_r} & \omega_{dq}-\omega_r \\ -\frac{1}{\sigma L_s}\omega_r & \frac{1}{\sigma L_s T_r} & -(\omega_{dq}-\omega_r) & -\frac{1}{\sigma T_s}-\frac{1}{\sigma T_r} \end{bmatrix} \quad ; \quad B=\begin{bmatrix} 1 & 0 \\ 0 & 1 \\ \frac{1}{\sigma L_s} & 0 \\ 0 & \frac{1}{\sigma L_s} \end{bmatrix} \quad U=\begin{bmatrix} V_{ds} \\ V_{qs} \end{bmatrix}$$

and: $T_r = \frac{L_r}{R_r}$; $\delta = 1-\frac{M^2}{\delta L_s L_r}$; $T_s = \frac{L_s}{R_s}$

III.5. Modeling of the centrifugal pump

The flow-head characteristic of a centrifugal pump can be approximated by quadratic form using *Pfleider–Peterman* model, in which the rotor speed x is a parameter:

$$H = a_0\omega^2 + a_1\omega\varphi + a_2\varphi^2 \tag{III-20}$$

With:

φ: The water flow (m³/s)

H: The total height (m)

ω: Rotation speed (rad/s)

a_0, a_1, a_2: are the coefficients given by the manufacturers.

The Q–H characteristic of the pipe network can be expressed by :

$$H = H_g + \psi\ \varphi^2 \tag{III-21}$$

ψ: is a constant which depends on conduit diameter and on all frictional losses of the pipe network.

H_g : is the geodesic height (m).

The centrifugal pump imposes a load torque proportional to the square of the speed of rotation of the motor which can be described by :

$$T = k_{pump} \cdot \omega^2 \tag{III-22}$$

k_{pump} : denotes the proportionality coefficient.

Knowing the performances of a centrifugal pump for the speed ω, the similarity laws make it possible to determine the performances for a speed ω' using the following relation:

$$\varphi' = \varphi \frac{\omega'}{\omega} \tag{III-23}$$

III.6 Modeling the voltage source inverter (VSI)

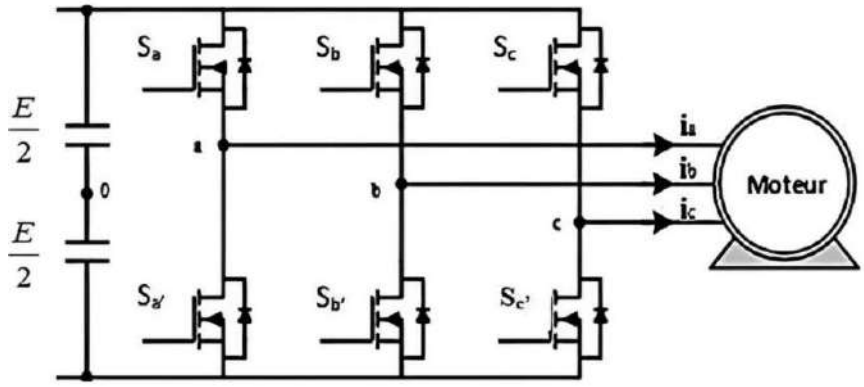

Fig III.6: Three-phase VSI fed star-connected induction machine.

The state of the switches, assumed to be perfect, can be defined by three boolean control S_i, with: i = a, b, c.

- If the upper transistor is conducting, the variables $S_i = 1$;

- If the lower transistor is conducting, the variables $S_i = 0$;

The simple voltages applied to the three stator phases are obtained from the following relationships taking into account the fictitious point "o". [36]

$$\begin{cases} V_{an} = V_{ao} + V_{on} \\ V_{bn} = V_{bo} + V_{on} \\ V_{cn} = V_{co} + V_{on} \end{cases} \tag{III-24}$$

By addition on a:

$$V_{an} + V_{bn} + V_{cn} = V_{ao} + V_{bo} + V_{co} + 3V_{on} \tag{III-25}$$

The system of the three-phase stator voltage is symmetrical there for:

$$V_{ao} + V_{bo} + V_{co} + 3V_{on} = 0 \tag{III-26}$$

Consequently, the following result emerges:

$$V_{on} = \frac{1}{3}(V_{ao} + V_{bo} + V_{co}) \tag{III-27}$$

By substituting equation (III-27) into the system of equation (III-24), the following result is obtained:

$$\begin{cases} V_{an} = \frac{1}{3}(2V_{ao} - V_{bo} - V_{co}) \\ V_{bn} = \frac{1}{3}(-V_{ao} + 2V_{bo} - V_{co}) \\ V_{cn} = \frac{1}{3}(-V_{ao} - V_{bo} + 2V_{co}) \end{cases} \quad \text{(III-28)}$$

After arranging the equations of the two systems, the following matrix system is obtained:

$$\begin{bmatrix} V_{an} \\ V_{bn} \\ V_{cn} \end{bmatrix} = \frac{1}{3} \cdot \begin{bmatrix} 2 & -1 & -1 \\ -1 & 2 & -1 \\ -1 & -1 & 2 \end{bmatrix} \cdot \begin{bmatrix} V_{ao} \\ V_{bo} \\ V_{co} \end{bmatrix} \quad \text{(III-29)}$$

with:

$$\begin{aligned} V_{ao} &= E.S_a \\ V_{bo} &= E.S_b \\ V_{co} &= E.S_c \end{aligned} \quad \text{(III-30)}$$

Finally, there exists:

$$\begin{bmatrix} V_{an} \\ V_{bn} \\ V_{cn} \end{bmatrix} = \frac{E}{3} \cdot \begin{bmatrix} 2 & -1 & -1 \\ -1 & 2 & -1 \\ -1 & -1 & 2 \end{bmatrix} \cdot \begin{bmatrix} S_a \\ S_b \\ S_c \end{bmatrix} \quad \text{(III-31)}$$

III.6.1 Sinusoidal PWM control strategy

To determine the closing and opening times of the switches, the PWM technique is used (PWM: pulse width modulation). The principle of the sinusoidal PWM control consists in comparing three reference voltages called modulating voltages to a high-frequency triangular signal called carrier (modulation wave). The reference signals are given by the following equation [37]:

$$\begin{cases} V_{sa_{ref}}(t) = r \cdot \frac{V_{dc}}{2} \sin(\omega_r t) \\ V_{sb_{ref}}(t) = r \cdot \frac{V_{dc}}{2} \sin(\omega_r t - \frac{2\pi}{3}) \\ V_{sc_{ref}}(t) = r \cdot \frac{V_{dc}}{2} \sin(\omega_r t + \frac{2\pi}{3}) \end{cases} \quad \text{(III-32)}$$

with: $\omega_r = 2\pi f_r$

Two parameters characterize the command:

The modulation index "m" equal to the ratio of the frequency of the carrier to the frequency of the reference:

$$m = \frac{f_p}{f_{ref}} \tag{III-33}$$

The voltage adjustment coefficient "r" equal to the ratio of the amplitude of the reference voltage to the peak value of the carrier:

$$r = \frac{V_{ref}}{V_p} \tag{III-34}$$

Our simulation diagram of the sinusoidal PWM control is illustrated by figure (III.7).

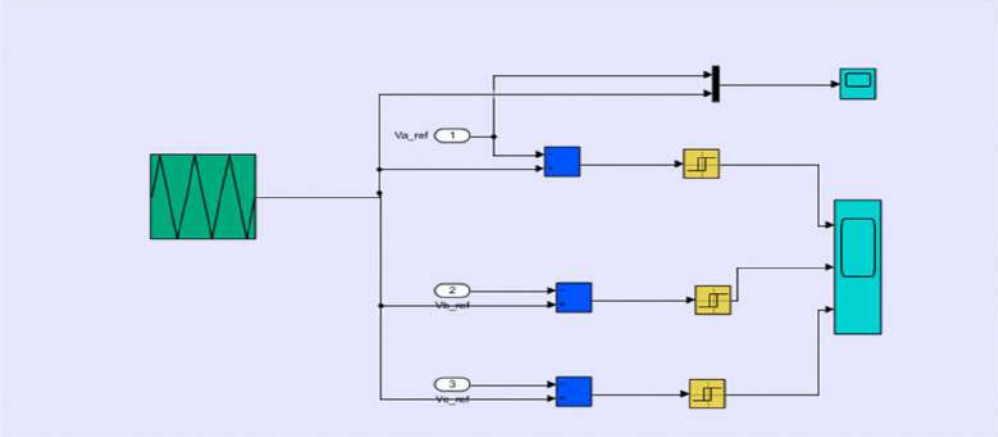

Fig III.7: Simulation diagram of the sinusoidal PWM control

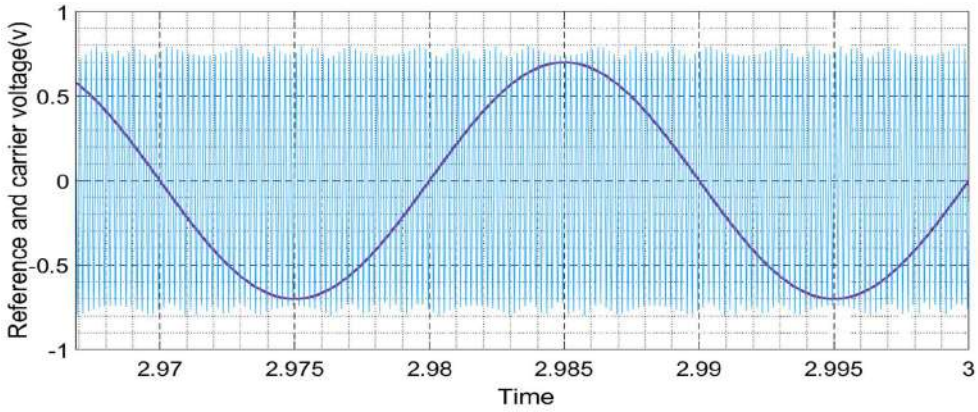

Fig III.8: Representation of the carrier and the modulator.

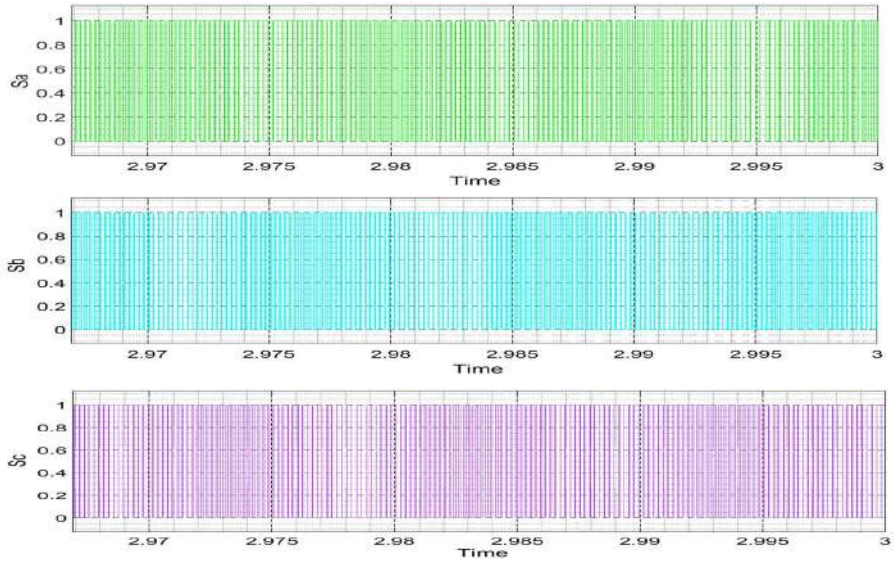

Fig III.10: Results of simulation of control signals.

III.7 Simulation of the induction motor

Figure III.11 presents the block diagram of the induction motor simulation developed using MATLAB/Simulink software. This simulation depicts the motor directly connected to a three-phase network with a line voltage of 220/380 V and a frequency of 50 Hz. The specific parameters employed for the induction motor model are detailed in the Appendix.

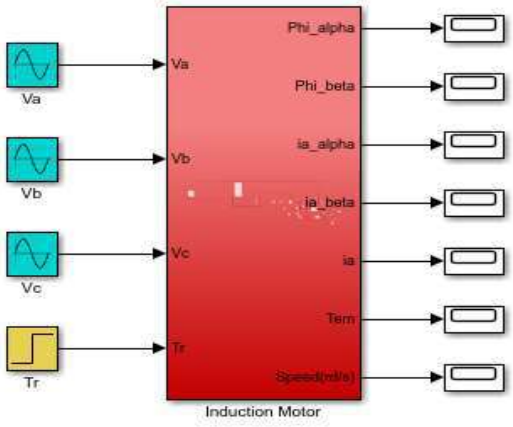

Fig III.11: Block diagram of induction motor simulation.

III.7.1 Simulation results

The simulation results represent the electrical and electromagnetic characteristics of the induction motor.

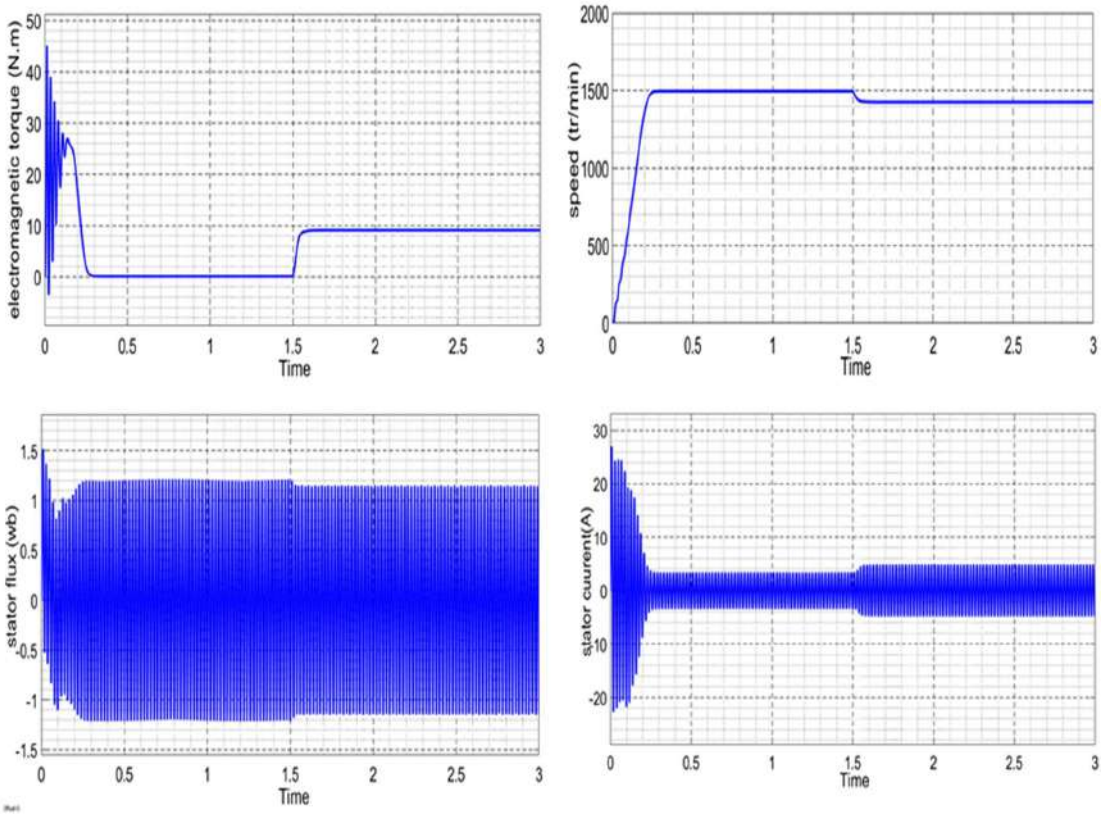

Fig III.12: Simulation of the induction motor for (T_r=9 Nm, t = 1.5 s)

III.7.2 Interpretations of the results

In this simulation, the motor behavior is illustrated through several key variables. The speed quickly rises to 1500 rpm, then slightly drops to around 1450 rpm at 1.5 seconds due to a load change. The electromagnetic torque starts with oscillations and reaches a peak value of 45 N.m, then stabilizes. At 1.5 seconds, it rises again to 9 N.m in response to the increased load. On the other hand, the stator flux shows regular oscillation within ±1.1 Wb and is not significantly affected by the load change. Regarding the stator current, it is high at startup, reaching ± 25 A, then drops to ± 5 A as the system stabilizes, and slightly increases again after 1.5 seconds due to the load rise.

III.7.3. Simulation of a Three-Phase Induction Motor with a DC/AC Inverter:

A DC/AC inverter is used to convert direct current (DC) into three-phase alternating current (AC) topower a three-phase induction motor. The inverter output terminals (Va, Vb, Vc) are connected to the motor's three input terminals. By controlling the inverter’s frequency and voltage, the motor’s speed and torque can be efficiently managed. This setup is commonly used in industrial applications where variable speed control is required.

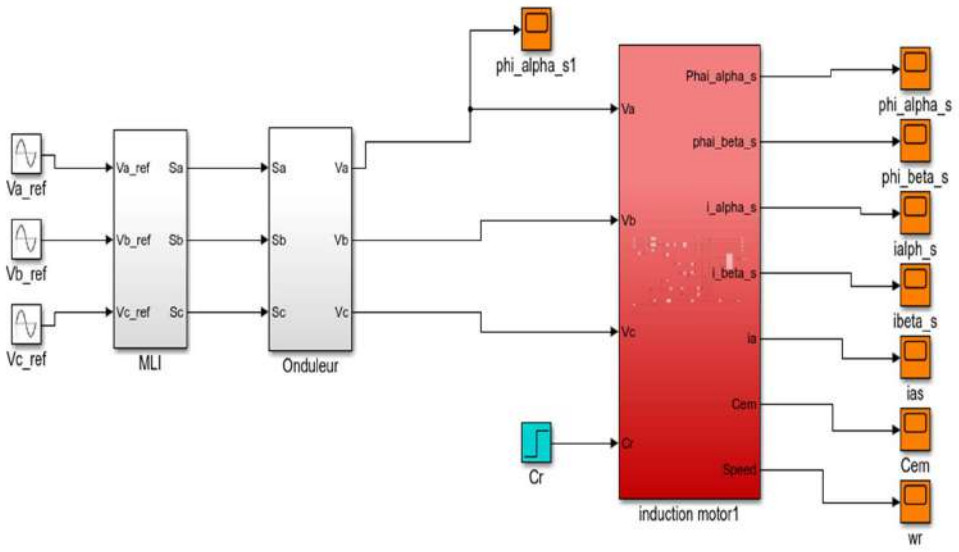

Fig III.13: Block diagram of induction motor with a DC/AC Inverter simulation.

III.7.4 Simulation results

The simulation results represent the electrical and electromagnetic characteristics of the induction motor.

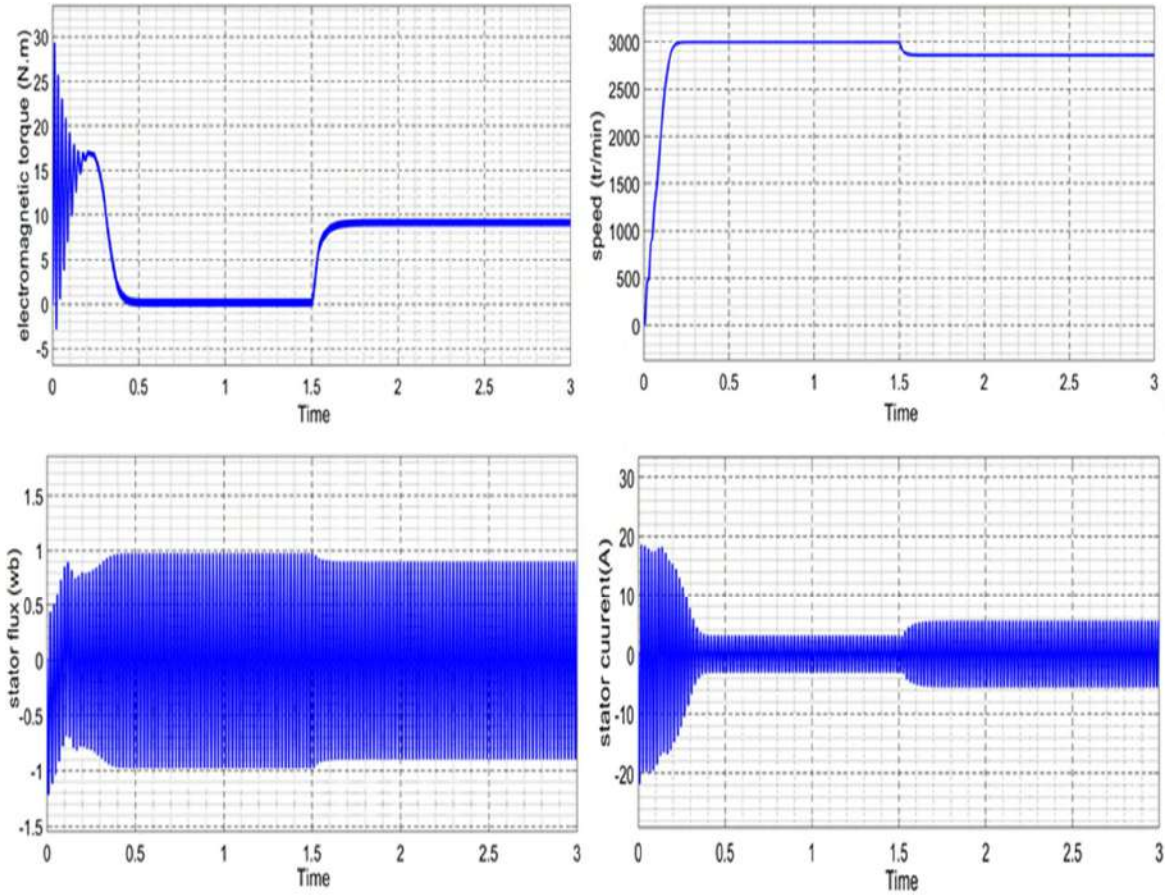

Fig III.6: Simulation of the induction motor for (Tr =9 Nm, t = 1.5 s)

III.7.6. Interpretations of the results

In this simulation, the motor's performance is analyzed through key indicators. The speed rapidly increases to 3000 rpm, then slightly drops to around 2850 rpm at 1.5 seconds due to a rise in load. The torque initially starts at 30 N.m, then decreases and stabilizes, before rising again to 9 N.m at 1.5 seconds as a response to the increased load. The stator flux maintains a steady oscillation within ±1 Wb throughout the simulation, showing stability regardless of load variation. As for the stator current, it begins at a high value of ± 20 A, then gradually decreases to ± 5 A, with a slight increase observed after 1.5 seconds due to the load change.

III.8. Conclusion

This chapter focused on the mathematical modeling of the core components in a solar photovoltaic water pumping system, including the induction motor (IM), centrifugal pump, and inverter.

The d-q reference frame transformation was applied to model the IM's electrical behavior. Additionally, a mathematical model was developed to describe the relationship between the hydraulic characteristics of the centrifugal pump, such as flow rate and pressure head, and its operational parameters, including rotational speed and motor torque. Finally, the chapter covered the mathematical modeling of the inverter, highlighting its role in converting the DC power from the photovoltaic system and boost converter into the AC voltage and frequency required to drive the IM.

Chapter IV.

Predictive Torque Control (PTC) of Induction Motor

IV.1 Introduction

The preceding chapter established the fundamental dynamic equations governing induction motor operation, which serve as the mathematical foundation for implementing Predictive Torque Control (PTC). As a model-based control strategy, PTC critically depends on accurate system representations of both the induction machine and power inverter dynamics. PTC derives its conceptual framework from Direct Torque Control (DTC) methodology, maintaining the core principle of electromagnetic torque and stator flux linkage regulation through optimal voltage vector selection.

This chapter relies on a mathematical model of the system to predict the future values of these variables, enabling the selection of the optimal switching state for the inverter based on a cost function optimization principle. The chapter will detail the general structure of the PTC algorithm, including the estimation of variables, prediction of torque and flux values, and the evaluation of the cost function to select the optimal voltage vector. To enhance the practical aspect, MATLAB/SIMULINK will be utilized to construct a model of an induction motor controlled by the PTC algorithm, with simulation results showcasing the effectiveness of this strategy in controlling a water pumping system.

IV.2 Fundamental Concept of Predictive Torque Control (PTC)

A general control scheme for Predictive Torque Control PTC applied to power converters and drives is presented in Figure IV.1. The power converter can be from any topology and number of phases, while the generic load shown in the figure can represent an electrical machine, the grid, or any other active or passive load. In this scheme measured variables $x(k)$ is used in the model to calculate predictions $x(k + 1)$ of the controlled variables for each one of the n possible actuations, switching states, voltages, or currents. Then these predictions are evaluated using a cost function which considers the reference values $x^*(k)$ and restrictions, and the optimal actuation S is selected and applied in the converter [35].

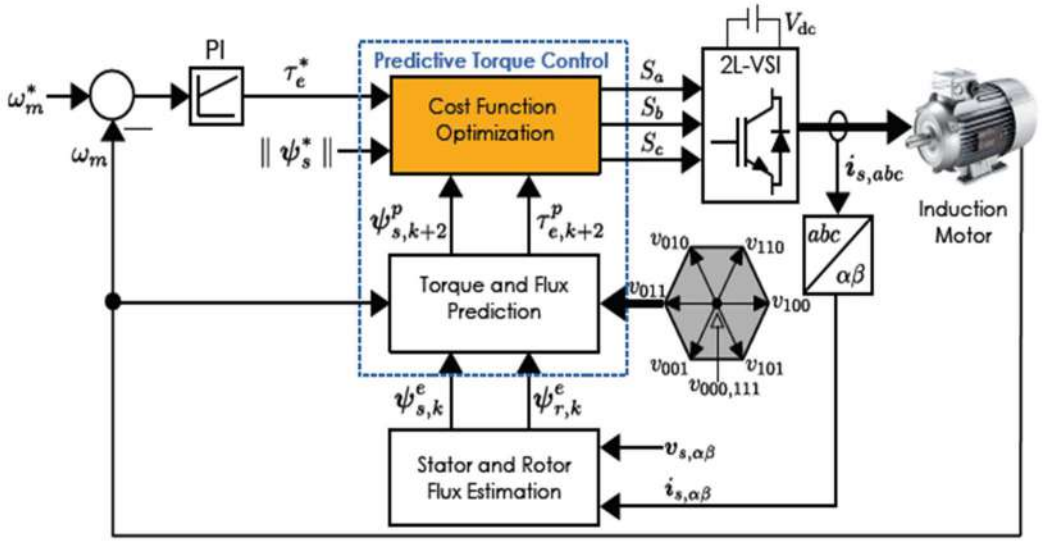

Fig IV.1: Block diagram of the PTC-based IM drive.

The two-phase stator currents and voltages ($i_{s,\alpha\beta}, v_{s,\alpha\beta}$) are measured to estimate the stator and rotor fluxes. The estimated stator flux is then used to calculate the electromagnetic torque. The reference torque (T_e^*)is generated by an external PI speed controller, while the stator flux reference is set to its nominal value. These values are used in the prediction block to compute future torque and flux values for all possible switching states. A cost function, which considers torque and flux errors, evaluates these predictions, and the optimal switching state is selected and applied to the inverter

IV.3 Estimation of Stator and Rotor Flux in PTC

In the PTC model shown in figure (IV.1), the stator and rotor flux estimation block, the values stator flux φ_s and the rotor flux φ_r is estimated at present sampling time.

IV.3 .1 Stator Flux Estimation

The estimation of stator flux $\hat{\varphi}_s(K)$ is carried out using the stator voltage equation. Predictive Torque Control (PTC) is modeled in the stationary reference frame, the angular speed is considered zero, which simplifies the equation.

$$v_s = R_s I_s + \frac{d\varphi_s}{dt} + j\omega_k \varphi_s \quad \text{(IV.1)}$$

So, the equation (IV.1) becomes

$$v_s = R_s I_s + \frac{d\varphi_s}{dt} \quad \text{(IV.2)}$$

The above equation is discredited using the Euler approximation method as follows:

$$\frac{d\varphi_s}{dt} = \frac{\varphi_s(K) - \varphi_s(K-1)}{T_s} \quad \text{(IV.3)}$$

where Ts is the sampling time period.

Now, using equation (IV.3) in equation (IV.2), we can obtain the estimated value of stator flux at present sampling time $\varphi_s(K)$.

$$\hat{\varphi}_s(k) = \hat{\varphi}_s(k-1) + T_s v_s(k) - R_s T_s i_s(k) \quad \text{(IV.4)}$$

IV.3.2 Rotor Flux Estimation

The estimation of rotor flux $\hat{\varphi}_r(k)$ is obtained from the flux linkage equations provided below.

$$\varphi_s = L_S i_S + L_m i_r \quad \text{(IV.5)}$$

$$\varphi_r = L_m i_S + L_r i_r \quad \text{(IV.6)}$$

By replacing i_r from equation (IV.5) in equation (IV.6) we obtain the rotor flux as:

$$\varphi_r = \frac{L_m}{L_r}\varphi_s + \left(L_m - \frac{L_S L_r}{L_m}\right) i_s \quad \text{(IV.7)}$$

The discretization of the above equation is done as:

$$\hat{\varphi}_r = \frac{L_m}{L_r}\hat{\varphi}_s + \left(L_m - \frac{L_S L_r}{L_m}\right) i_s \quad \text{(IV.8)}$$

IV.4 Predictive torque and flux control

Based on the applied stator voltage vector $u_{si}(k)$, the measured stator current $i_s(k)$, and the estimated stator flux $\varphi_s(k)$at the current sampling instant, it is possible to obtain one-step-ahead predictions of the stator current $i_s(k+1)$, and the stator flux $\varphi_s(k+1)$.

The predicted values of torque and stator flux are then used to evaluate a cost function F, which aims to minimize the quadratic error between the predicted values and their respective references. The switching state that yields the minimum value of this cost function is selected to be applied to the machine terminals in the next sampling interval, following the principle of receding horizon control.

Assuming that a first-order approximation of the derivatives is appropriate, given the first-order dynamics inherent in the state-space representation of the induction motor model, the following expressions can be formulated:

$$\dot{x} = \frac{x(K+1) - x(K)}{T_s} \quad \text{(IV.9)}$$

Where T_s denotes the sampling period, the one-step-ahead predictions of stator flux, stator current, rotor flux, and electromagnetic torque can be obtained using standard estimation techniques from the previous sampling instant, as follows:

$$i_{sa}(K+1) = (1 - \gamma T_s) i_{sa}(K) + T_s \left(\frac{K}{T_r}\varphi_{ra}(K) + K\varphi_{r\beta}(K) + \frac{u_{sa}(K)}{\sigma L_S}\right) \quad \text{(IV.10)}$$

$$i_{s\beta}(K+1) = (1 - \gamma T_s) i_{s\beta}(K) + T_s \left(-\omega\varphi_{ra}(K) + \frac{K}{T_r}\varphi_{r\beta}(K) + \frac{u_{s\beta}(K)}{\sigma L_S}\right) \quad \text{(IV.11)}$$

$$\varphi_{s\alpha}(K+1) = \varphi_{sa}(K) + T_s u_{sa}(K) - R_s T_s i_{sa}(K) \quad \text{(IV.12)}$$

$$\varphi_{s\beta}(K+1) = \varphi_{s\beta}(K) + T_s u_{s\beta}(K) - R_s T_s i_{s\beta}(K) \quad \text{(IV.13)}$$

Where the total magnetic leakage factor is $\sigma=1-L_m^2/L_sL_r$.

The predicted value for torque is deduced by:

$$T_e(K+1) = p(\varphi_{sa}(K+1)i_{s\beta}(K+1) - \varphi_{s\beta}(K+1)i_{s\alpha}(K+1)) \quad \text{(IV.14)}$$

Prediction of the value of the electromagnetic torque can be obtained using the predicted values of the stator flux and stator current:

$$T_e[k+1] = \frac{3}{2p}\left(\varphi_{sa}[k+1]i_{s\beta}[k+1] - \varphi_{s\beta}[k+1]i_{s\alpha}[k+1]\right) \quad \text{(IV.15)}$$

IV.5 Cost Function Minimization

In Predictive Torque Control (PTC), the predicted variables are assessed using a predefined cost function that facilitates the selection of the optimal switching state. This cost function typically incorporates the absolute difference between the reference values and the predicted responses [36]. The cost function formulated for the predictive torque control of an induction machine is expressed as follows:

$$g = \left|T_e^*(k+1) - T_e^p(k+1)\right| + \lambda_\varphi \left|\varphi_s^*(k+1) - \varphi_s^p(k+1)\right| \quad \text{(IV.16)}$$

where $T_e^*(k+1)$ and $\varphi_s^*(k+1)$ are reference electromagnetic and stator flux values. $T_e^p(k+1)$ and $\varphi_s^p(k+1)$ are predicted values of electromagnetic and stator flux at (k+1) time instant. λ_φ is the weighting factor which helps in increasing or decreasing the relative importance of stator flux with respect to electromagnetic torque. The value of the weighing factor is taken as nominal values of torque and stator flux.

$$\lambda_\varphi = \frac{T_n}{|\phi_{sn}|} \quad \text{(IV.17)}$$

The cost function g is evaluated for each possible voltage vector. The voltage vector that yields the minimum cost is selected, and its corresponding switching state is applied to the three-phase inverter.

IV.6 General structure of PTC

Figure (IV.2) illustrates the predictive torque control (PTC) strategy applied to an induction motor. In this approach, the performance of the drive system largely depends on the accurate selection of the cost function and the prediction model. Proper formulation of the cost function—along with appropriate weighting factors is critical to ensure precise torque and flux regulation, minimize

switching losses, and achieve dynamic performance comparable to or superior to conventional methods such as DTC.

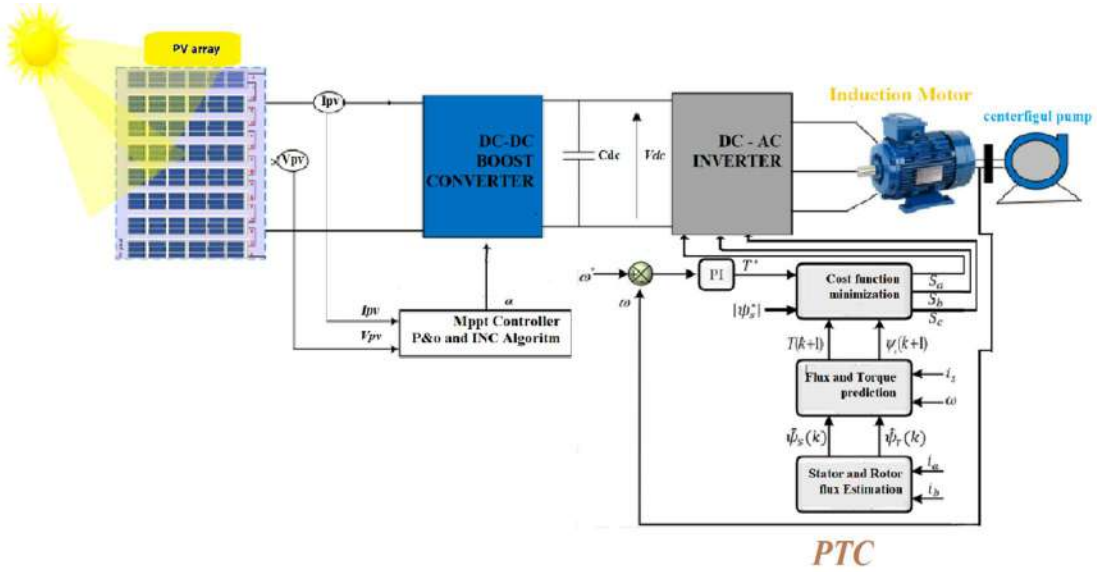

Fig IV.2 Structure of the predictive torque control of the water pumping system.

IV.7 Advantages and disadvantages of PTC

IV.7.1 Advantages

- Fast torque and flux response: PTC provides rapid dynamic response by predicting system behavior and selecting optimal switching states in real time.
- High efficiency at variable speeds: maintains efficient performance under varying load and speed conditions.
- No modulation stage required: eliminates the need for PWM or SVM, as control is directly applied through inverter switching states.
- Reduced torque and flux ripple: with accurate prediction and cost function tuning, PTC minimizes torque and flux pulsations.
- Inherent constraint handling: allows easy integration of system constraints (current and voltage limits) within the control algorithm.
- Good performance without PI controllers: no need for PI current regulators, reducing the complexity of gain tuning.

IV.7.2 Disadvantages

- High computational load: Real-time prediction and optimization increase the demand on the digital signal processor (DSP) or controller.

- Model sensitivity: control performance is highly dependent on the accuracy of the motor model parameters.
- Variable switching frequency: unlike fixed-frequency methods, switching frequency varies, complicating EMI filtering and inverter design.
- Tuning complexity: requires careful tuning of weighting factors in the cost function to balance torque, flux, and switching effort [40].

IV.8 Simulation diagram

Figure IV.3 illustrates the *MATLAB/SIMULINK* block-diagram used to simulate Predictive Torque Control of the induction motor.

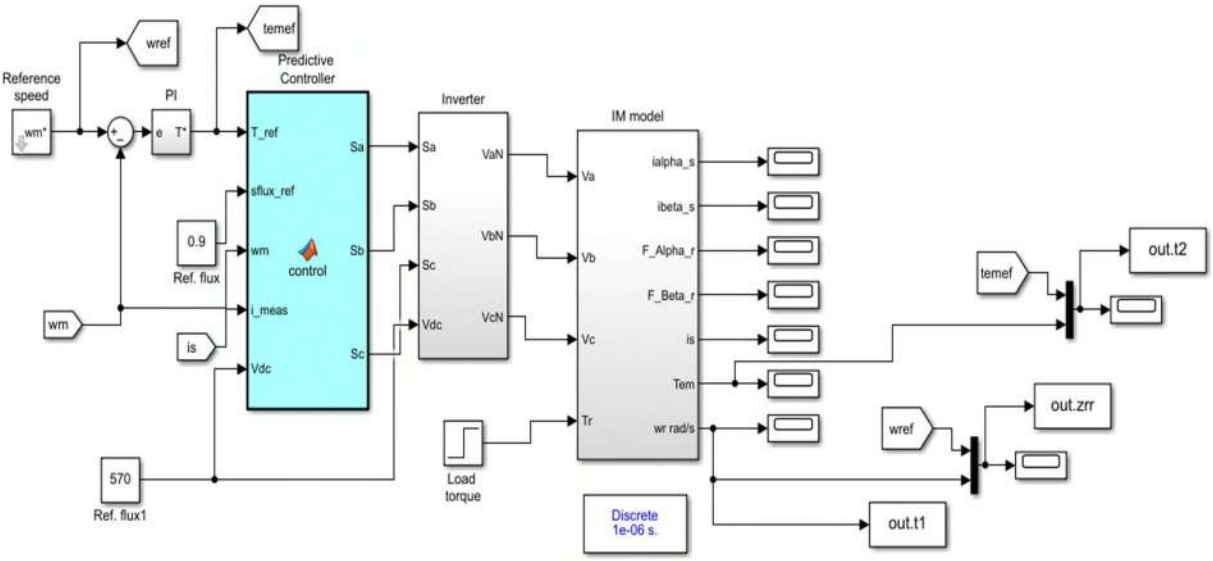

Fig IV.3: Block diagram Simulink of PTC

IV.9 Simulation results

The Predictive Torque Control (PTC) strategy was simulated using MATLAB/Simulink for a three-phase induction motor rated at 1.5 kW, with motor parameters detailed in the appendix. The system's performance was evaluated during both the start-up transient and steady-state conditions. To assess dynamic behavior, a sudden step change in load was introduced, and the resulting torque and flux responses were observed and analyzed.

IV.9.1 Simulation results for a speed reversal

To evaluate the robustness of the Predictive Torque Control scheme, Figure (IV.4) presents simulation results of the control system response to both load torque and reference speed reversals. The load torque applied to the motor (+5 Nm) at 0.5 seconds. Meanwhile, the reference speed command

undergoes a reversal from (100 rad/s to -100 rad/s) at 1.0 second. The results demonstrate the controller's ability to quickly adapt to sudden changes in both torque and speed, indicating high system efficiency and stability.

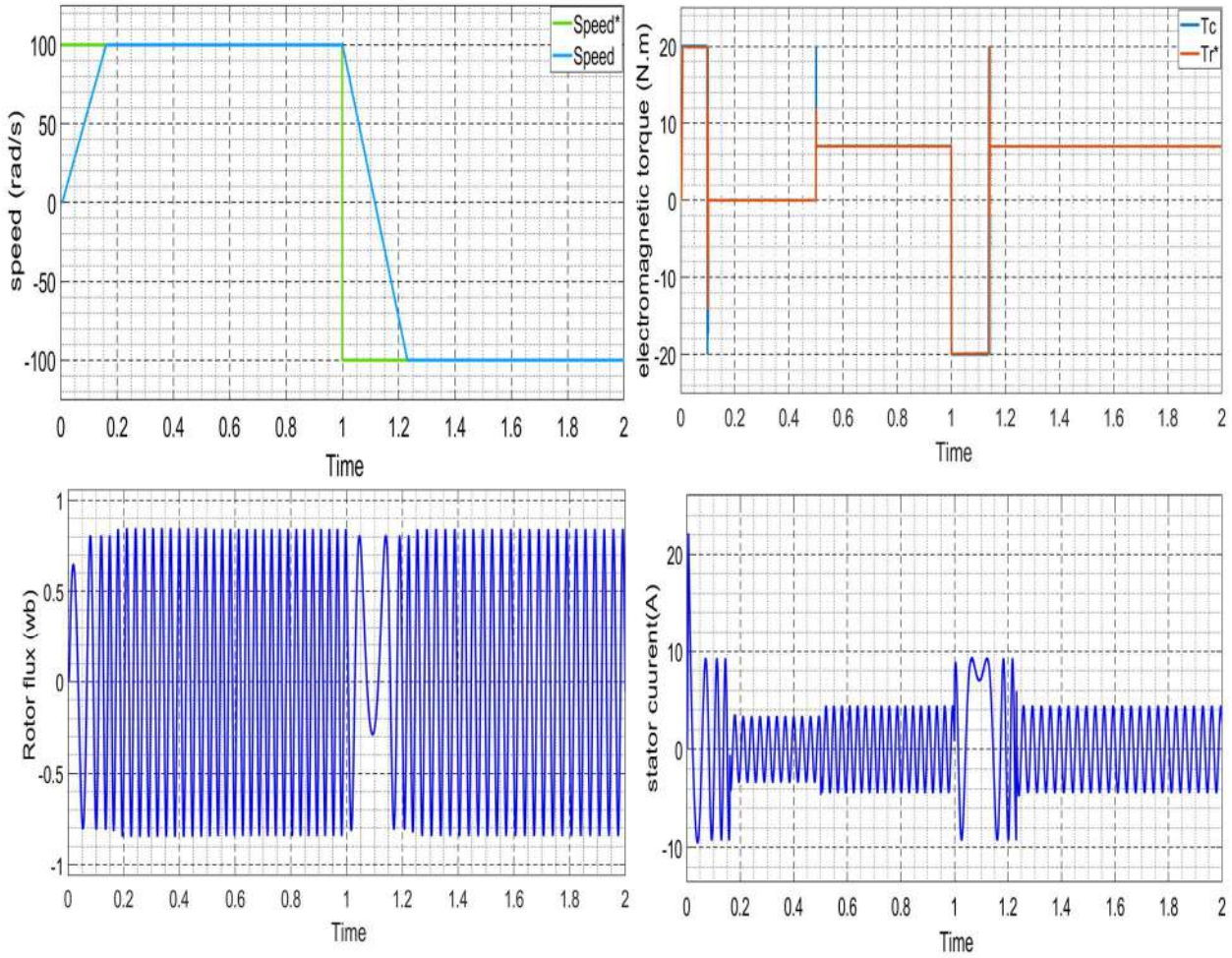

Fig IV.4: Simulation results of the PTC for a speed reversal.

IV.10.2 Simulation results at low speed

To further assess the effectiveness of the Predictive Torque Control (PTC) scheme, the presented simulations illustrate the system's dynamic performance under low-speed operation and during reference speed reversal. The results confirm the controller's ability to maintain stable torque and flux behavior while ensuring fast and accurate speed tracking, even under challenging operating conditions.

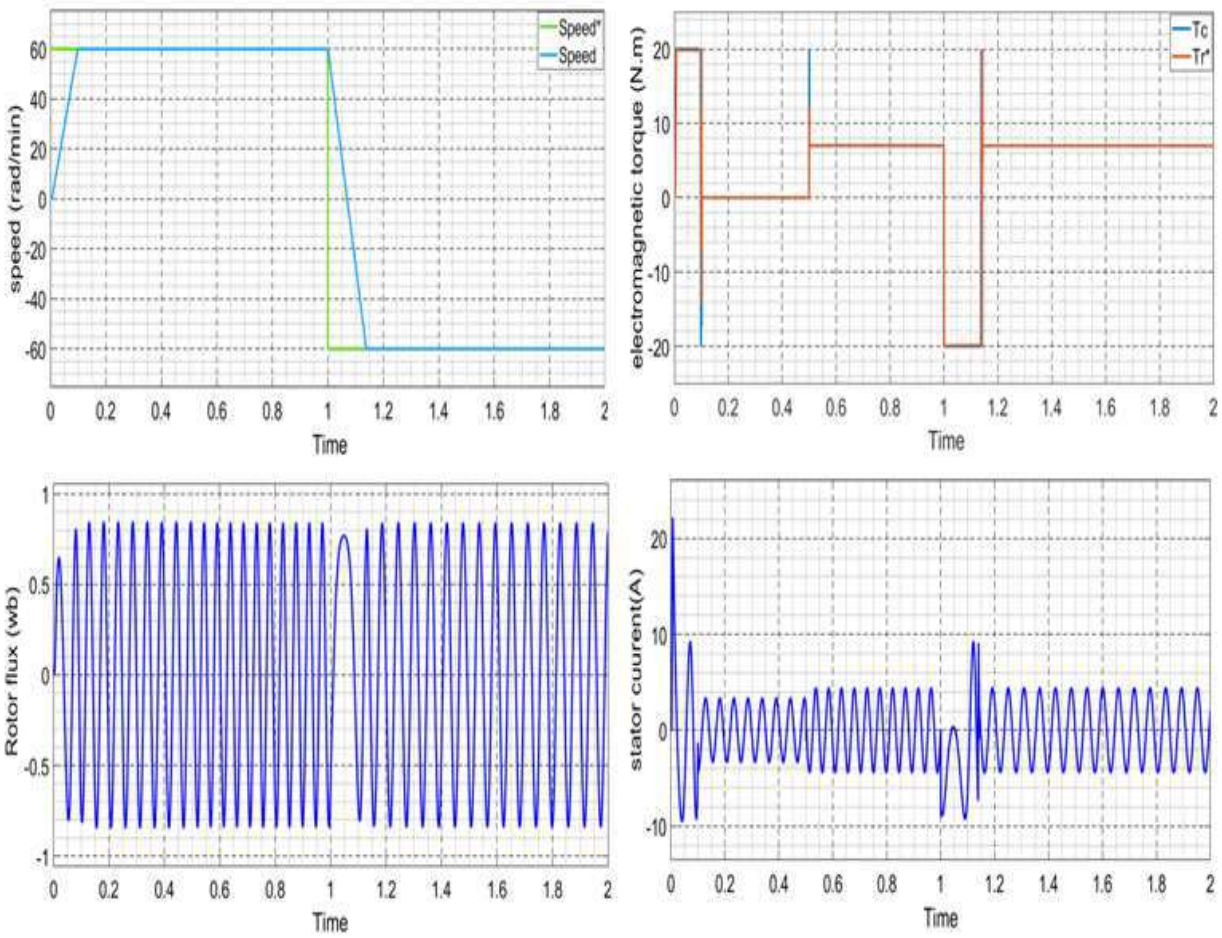

Fig IV.5: Simulation results of the PTC at low speed.

IV.11 Simulation the PV pumping system

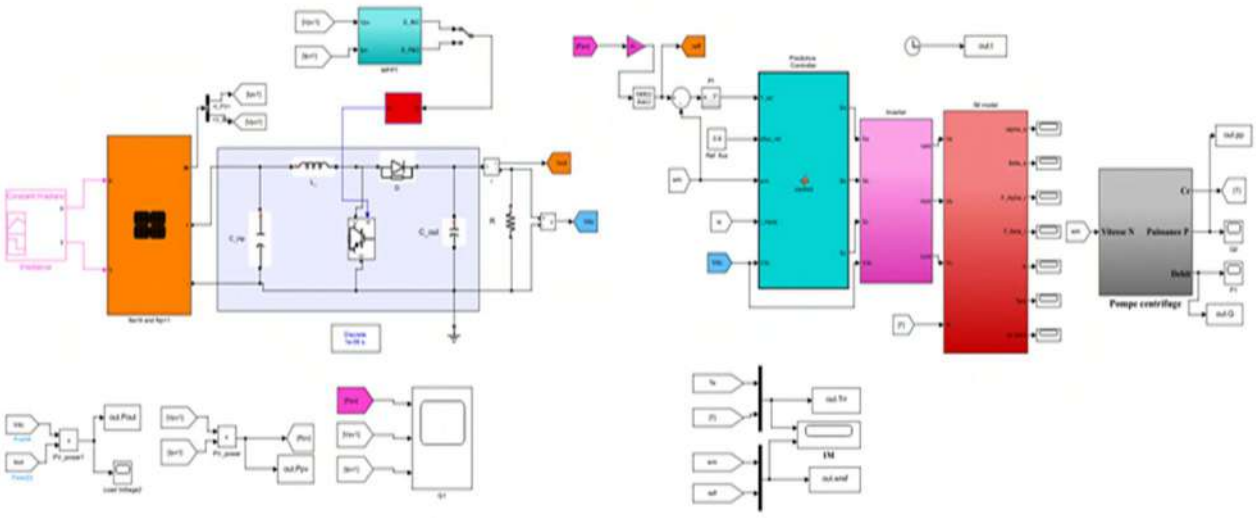

Fig IV.6: Simulation design of the photovoltaic water pumping system

IV.11.1 Simulation results at variable irradiance

❖ **P&O method**

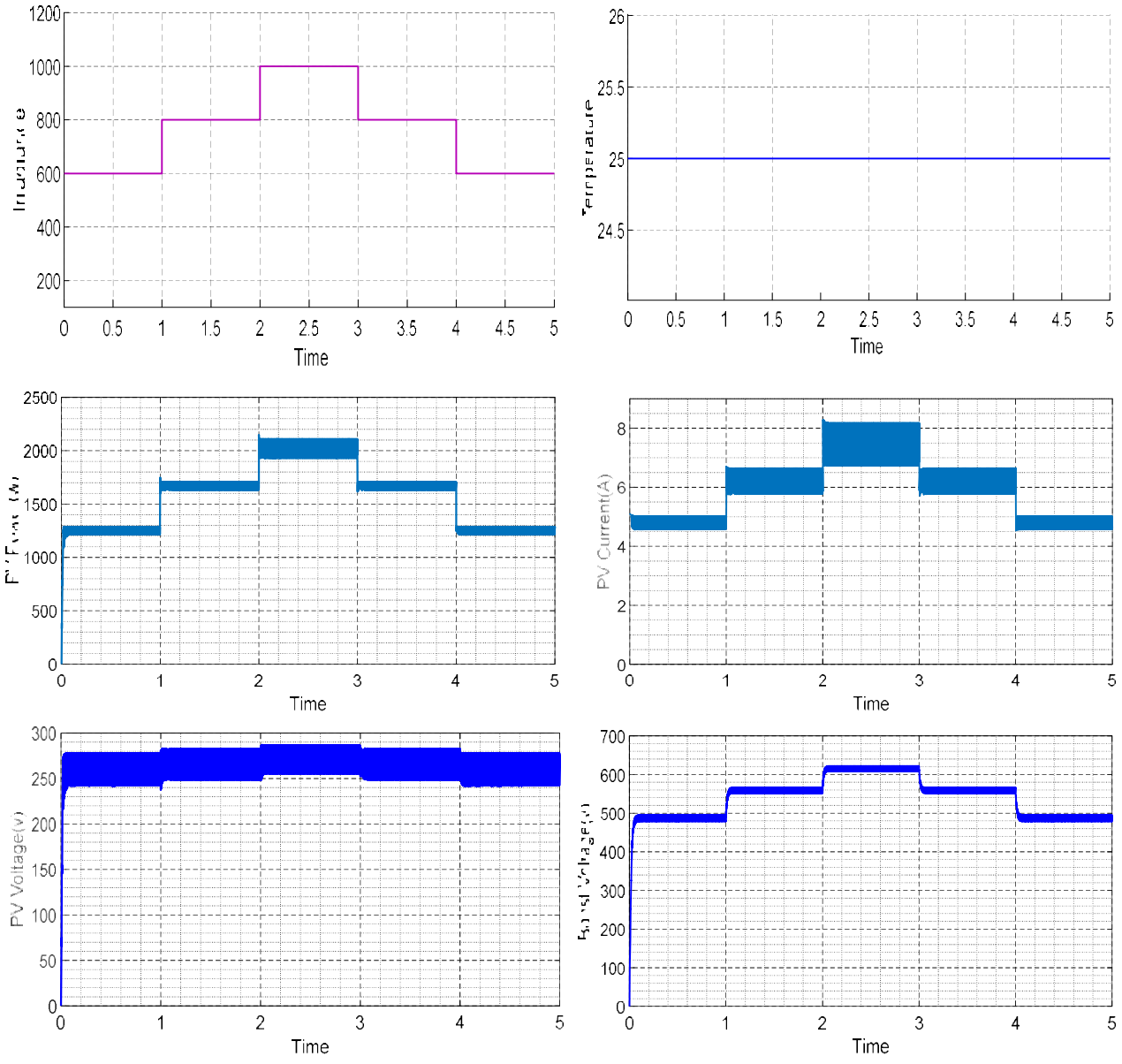

Fig IV.7: PV and Boost characteristics at variable Irradiance.

In the figure IV.7, the simulation results at a constant temperature of 25°C and varying irradiance show that the P&O algorithm performs efficiently in tracking the maximum power point (MPP). The power and current responded quickly to each change in irradiance without noticeable oscillations. Additionally, the output voltage from the PV panels and the boost converter remained stable and proportional to the generated power, indicating system stability and fast dynamic response. This confirms the effectiveness of the algorithm in accurately and rapidly tracking the optimal operating point under varying irradiance conditions.

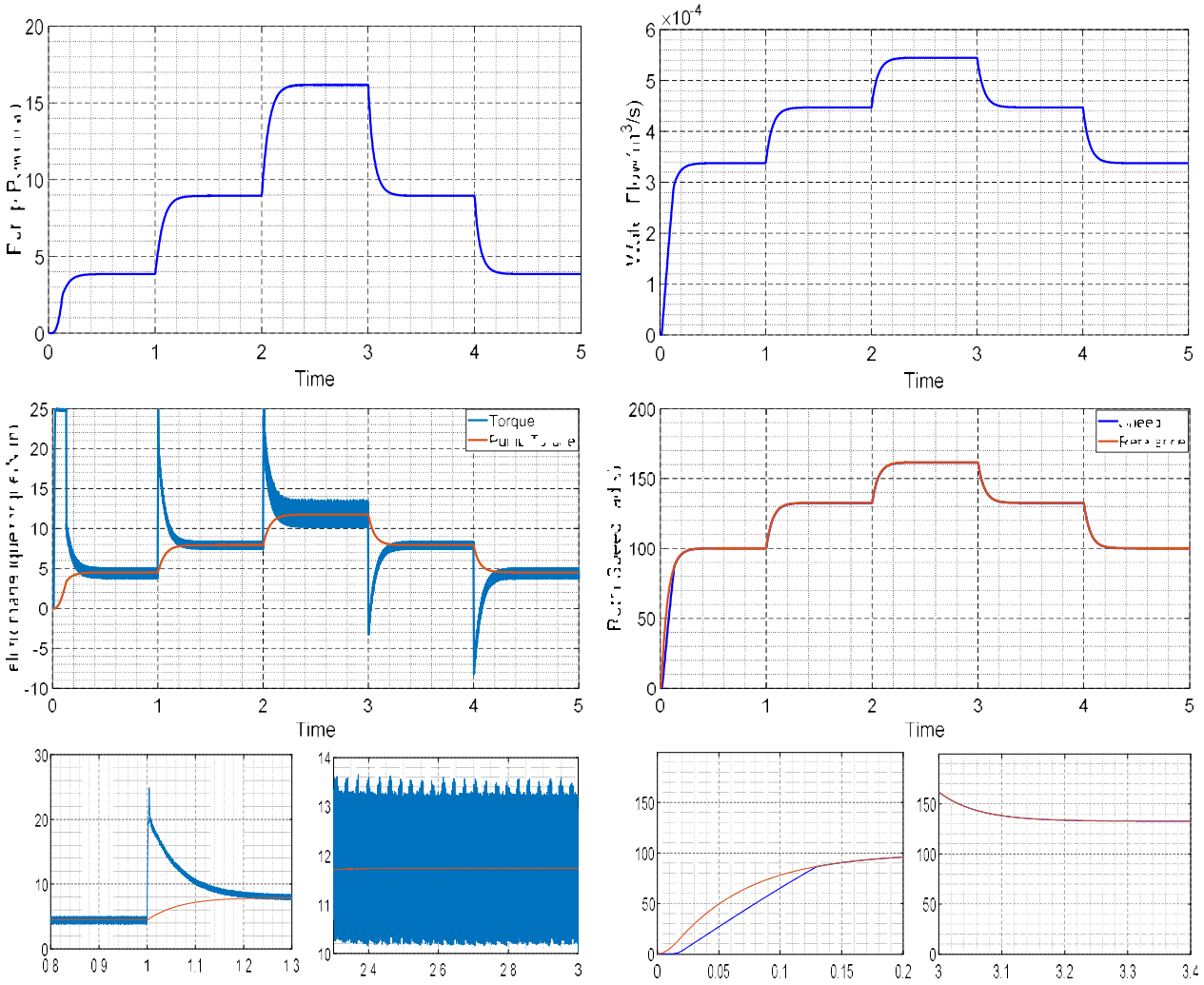

Fig IV.8: Motor-pump characteristics at variable Irradiance

The simulation results in Fig IV.8 demonstrate stable and efficient performance of the motor-pump system under variable solar irradiance at a constant temperature of 25°C.

Pump power increases gradually as irradiance rises, then drops when irradiance decreases. Water flow rate follows a similar pattern, indicating a direct relationship between solar input and hydraulic output. The electromagnetic torque peaks during irradiance transitions and stabilizes between 10 and 15 Nm, aligning well with the pump torque, which shows a fast dynamic response.

Rotor speed increases from 100 rad/s to 160 rad/s and remains close to the reference value, confirming the accuracy of the control system., the system operates smoothly and reliably under varying solar conditions, with consistent coordination between power, flow, torque, and speed, demonstrating the effectiveness of the photovoltaic-driven motor-pump configuration.

❖ INC method

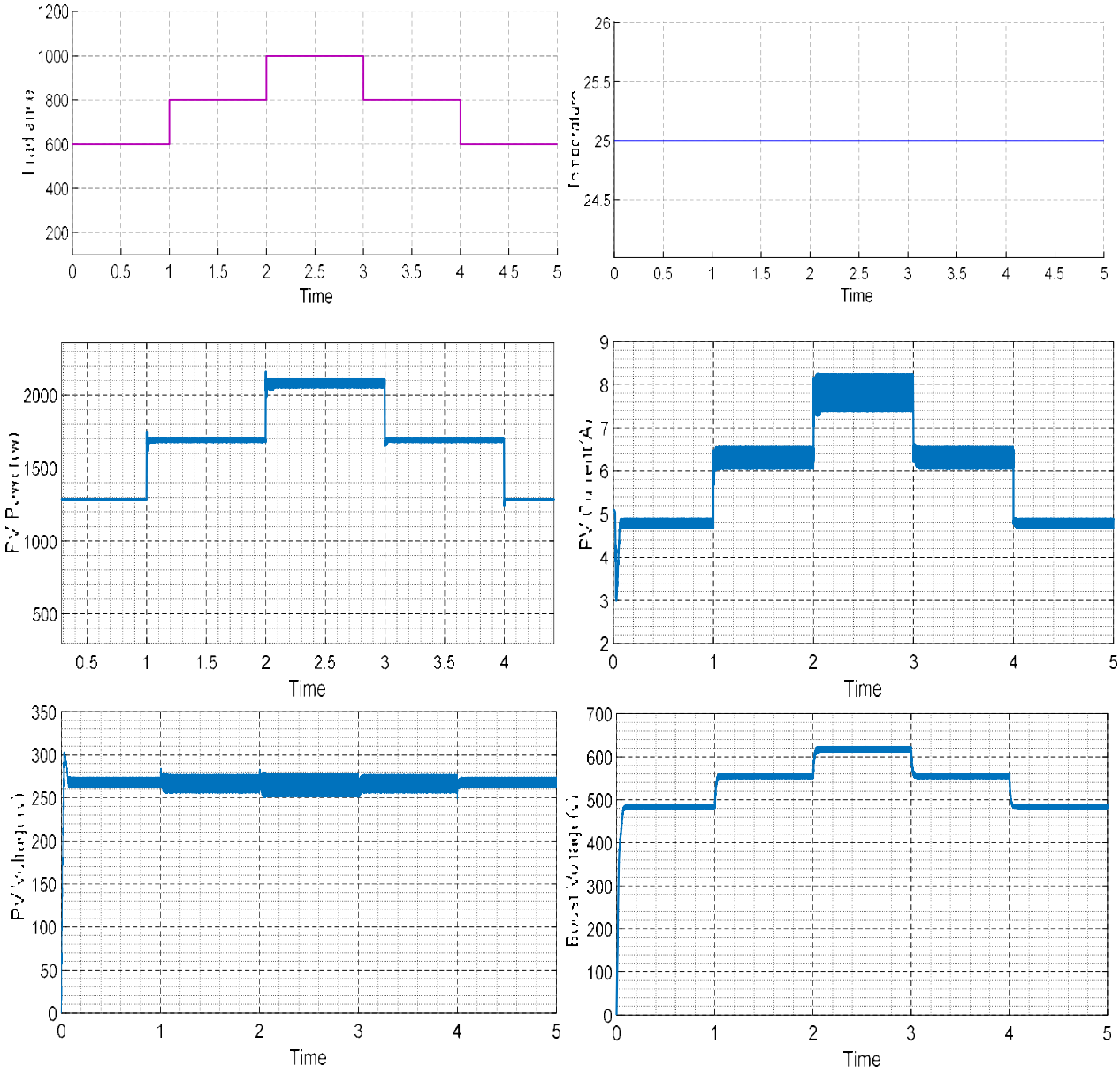

Fig IV.9: PV and Boost characteristics at variable Irradiance

The simulation results in Fig IV.9 illustrate the dynamic performance of the photovoltaic (PV) system and the boost converter under variable irradiance using the INC-MPPT algorithm.

As shown in the top left graph, irradiance increases from 600 to 1000 W/m² and then decreases to 600 W/m², while the temperature remains constant at 25°C. In response, the PV output power rises proportionally, demonstrating the INC algorithm's effectiveness in tracking the maximum power point (MPP). Similarly, PV current increases from approximately 3.5 A to 8 A, while the PV voltage remains nearly constant, indicating a stable operating point.

The boost converter output voltage adapts accordingly, reflecting efficient power conversion. Overall, the results confirm the INC algorithm's capability to accurately and rapidly track the MPP under varying irradiance, ensuring voltage stability and coordinated performance between the PV array and the boost converter.

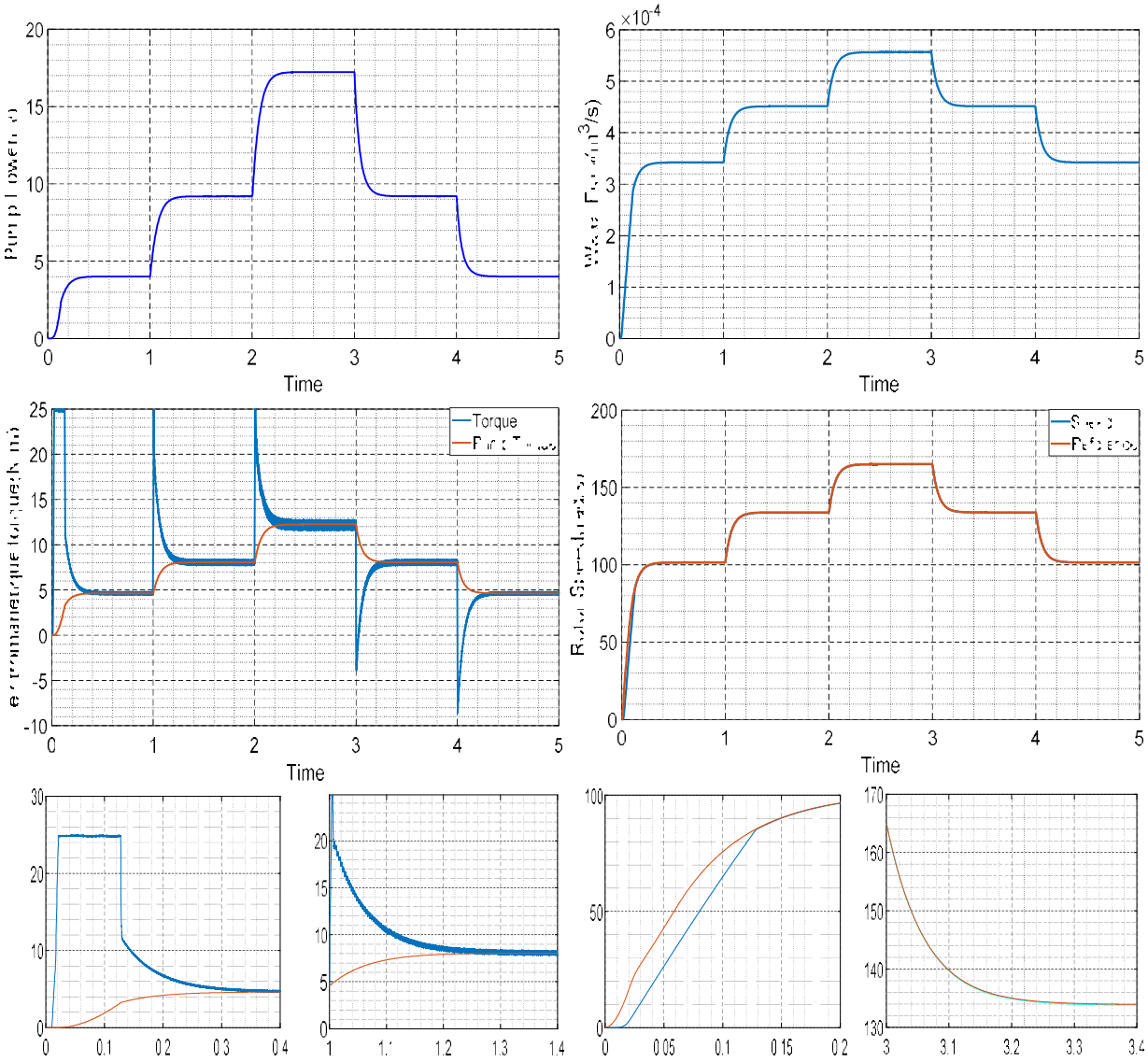

Fig IV.10: Motor-pump characteristics at variable Irradiance

The results in Fig IV.10 demonstrate stable and efficient performance of the motor-pump system using the Incremental Conductance (INC) algorithm under variable irradiance and constant temperature of 25°C.

The pump power increases as irradiance rises from 600 to 1000 W/m², then decreases when irradiance drops to 600 W/m². The water flow rate also increases, showing a direct correlation with the available

solar power. The electromagnetic torque responds quickly to irradiance transitions and stabilizes between 10 and 15 Nm in line with the pump torque.

The rotor speed rises gradually from 100 to 160 rad/s and closely follows the reference speed throughout. These results confirm the effectiveness of the INC algorithm in accurately and rapidly tracking the maximum power point (MPP), ensuring coordinated behavior between voltage, current, and power, and achieving high efficiency in photovoltaic water pumping applications.

IV.12 Conclusion

This chapter introduced the fundamental concepts of Predictive Torque Control (PTC) and explored its application through simulation in a photovoltaic water pumping system driven by an induction motor. The simulation outcomes indicate that PTC represents an effective alternative to traditional control strategies, particularly in addressing issues related to fluctuations in solar irradiance and load torque. PTC is distinguished by its fast dynamic response and model-based predictive approach, which contribute to enhanced system performance under changing operating conditions. Future studies may focus on fine-tuning PTC parameters to further improve the overall efficiency and reliability of photovoltaic pumping systems.

General Conclusion

This study focuses on the modeling and simulation of a photovoltaic water pumping system designed to supply water to remote areas lacking access to conventional energy sources. The photovoltaic generator was modeled and simulated using MATLAB under different irradiance and temperature levels to examine their impact on overall system performance. The study specifically investigated the effectiveness of Predictive Torque Control (PTC) as a motor control strategy for the induction motor driving the pump.

Additionally, two Maximum Power Point Tracking (MPPT) algorithms Perturb and Observe (P&O) and Incremental Conductance (INC)—were implemented and integrated with the PTC-based control structure to enhance the energy extraction process from the photovoltaic source.

The main objective of this thesis was to evaluate the robustness and dynamic performance of PTC in the context of photovoltaic pumping applications. A series of simulation tests were conducted under varying environmental conditions to assess the system's stability and responsiveness. The results confirm that PTC offers fast torque response, precise control, and high efficiency, even in the presence of fluctuations in solar irradiance and temperature. These findings highlight PTC as a promising and reliable control strategy for improving the performance and durability of photovoltaic water pumping systems operating in real-world, variable environments.

References

[1]. C.Cabal, "Optimisation énergétique de l'étage d'adaptation électronique dédie à la conversion photovoltaïque ", Université De Toulouse,2003.

[2]. Trishan esram, Patrick L. Chapman, "Comparison of photovoltaic array maximum power point tracking", IEEE, 2007.

[3]. G.F. Tchokcth, "Commande des hacheurs MPPT par la logique floue", Mémoire De Magister, Enp,2006.

[4]. M. E. Elhawary, "Electric Power Application of Fuzzy Systems", IEEE Press,1998.

[5]. Belhadj Mohammed, "Modélisation d'un système de captage photovoltaïque autonome", centre universitaire de Bechar, Institut des Sciences Exactes.

[6]. A. HADJ ARAB, M. BENGHANEM and A. GHARBI. Dimensioning of Photovoltaic Pumping Systems. Review of Renewable Energies. vol.8, pp (19 – 26), 2005.

[7]. A, Oi. Design And Simulation of Photovoltaic Water Pumping System. these doctorate California Polytechnic. California: University San Luis Obispo, 2005.

[8]. J, Royer and T, Djako. Course Manual for Engineers and Technicians, Photovoltaic Pumping. S.L.: University Of Ottawa, 2002.

[9]. J. Royer, J. Djiako, E. Schiller Et B. Sada « Le Pompage Photovoltaïque » Manuel de cours à l'intention des ingénieurs et des techniciens IEPF/Université d'Ottawa/ EIER/CREPA, 1998.

[10]. V. Salas, E. Olias, A. Barrado, A. Lazaro. Review of the maximum power point tracking

[11]. algorithms for stand-alone photovoltaic systems. Solar energy materials solar cells. vol 90,

[12]. pp. 1555-1578, 2006;

[13]. Boylestad, R.L.; Nashelsky, L. Electronic Devices and Circuit Theory; Pearson Educación: London, UK, 2002.

[14]. M. F. Habbati Bella, Ramdani Youcef, "A detailed modeling of photovoltaic module using matlab," NRIAG journal of Astronomy and Geophysics, 2014.

[15]. H.-L. Tsai, C.-S. Tu, and Y.-J. Su, "Development of generalized photovoltaic model using matlab/simulink," in Proceedings of the World Congress on Engineering and Computer Science San Francisco, USA, 2008.

[16]. J. Hernanz, J. Martin, I. Z. Belver, J. Lesaka, E. Guerrero, and E. P. Perez, "Modelling of photovoltaic module," in International Conference on Renewable Energies and Power Quality (ICREPQ10) Granada (Spain), 2010.

[17]. T.-F. Wu et Y.-K. Chen, Modeling PWM DC/DC converters out of basic converter units, IEEE Trans. Power Electron., vol. 13, no 5, p. 870–881, 1998.

[18]. A. Safari and S. Mekhilef, "Simulation and Hardware implementation of incremental conductance MPPT with direct control method using Cuk converter", IEEE Trans.Ind. Electron., vol . 58, no. 4, Apr. 2011, pp. 1154-1161

[19]. Geetanjali Manekar and al. Modeling Methods of Three Phase Induction Motor, National Conference on Innovative Paradigms in Engineering & Technology (NCIPET- 2013)

[20]. A. Meroufel, Decoupled control of an asynchronous machine without mechanical sensor, Doctoral thesis, Djillali Liabes University Of Sidi-BelAbbès, 2004.

[21]. S. Barkat . Study of the voltage inverter-asynchronous motor association. University of Mohamed Boudiaf M'sila. 2020.

[22]. Bakolia, A. (2021). Model Predictive Control of the Induction Motor: A Project Report. Master of Technology, Department of Electrical Engineering, Indian Institute of Technology Madras. July 2021

[23]. Kennel, R. (2010). High Performance Speed Control Methods for Electrical Machines: An Assessment. Page 3,4.

[24]. Vargas, R., Ammann, U., & Kouro, S. (2007). Predictive Torque Control of an Induction Machine Based on State Space Models.

[25]. Zhang, Y., Li, X., & Wang, H. (2020). A Three-Vector Model Predictive Torque Control Strategy for Induction Motors to Reduce Current Harmonics. Page 112–118.

[26]. Chen, L., H. Xu, X. Sun, and Y. Cai, \Three-vector-based model predictive torque control for a permanent magnet synchronous motor of EVs," IEEE Transactions on Transportation

[27]. Electri_cation, Vol. 7, No. 3, 1454{1465, Sept. 2021, doi: 10.1109/TTE.2021.3053256.

[28]. Djamel, M. (2021). Enhanced Finite-State Predictive Torque Control of Induction Motor. Przegląd Elektrotechniczny, 97(4), 43–47.

[29]. Jean Thomas, Anders Hansson, “Speed Tracking of a Linear Induction Motor - Enumerative Nonlinear Model Predictive Control,” arXiv preprint arXiv:1209.1114, Sep. 2012.

Appendix

A. Induction motor parameters :

IM	Values
Nominal power (P) [KW]	1.5
Rated speed(Ω) [rpm]	1420
Nominal frequency (f) [Hz]	50
Stator resistor (Rs) [Ω]	4.850
Rotor resistor (Rr) [Ω]	3.805
Stator inductor (Ls) [H]	0.274
Rotor inductor (Lr) [H]	0.274
Mutual inductor (M) [H]	0.258
Number of pole pairs (P)	2
Rated voltage [V]	20

B. Parameter values of the boost converter:

Boost converter parameters	Values
V_{dc}	600 V
C_1	100 µF
C_2	100 µF
L	3 mH

C. PV Parameters :

Parameters of the PV cell	Values
Maximum power (P_{mpp})[W]	235
Maximum current (I_{mpp})[A]	7.99
Maximum voltage (V_{mpp})[V]	29.42
Open circuit voltage (V_{oc})[V]	36.96
Short circuit current (I_{cc})[A]	8.48